Fetal estrogens are not involved in sex determination but critical for early ovarian differentiation in rabbits

Geneviève Jolivet, Nathalie Daniel-Carlier, Erwana Harscoët, Eloïse Airaud, Aurélie Dewaele, Cloé Pierson, Frank Giton, Laurent Boulanger, Nathalie Daniel, Béatrice Mandon-Pépin, et al.

Endocrinology, 2022, Vol. 163, No. 1, 1–22
https://doi.org/10.1210/endocr/bqab210
Research Article

Research Article

Fetal Estrogens are not Involved in Sex Determination But Critical for Early Ovarian Differentiation in Rabbits

Geneviève Jolivet,[1] Nathalie Daniel-Carlier,[1] Erwana Harscoët,[1] Eloïse Airaud,[1] Aurélie Dewaele,[1] Cloé Pierson,[1] Frank Giton,[2] Laurent Boulanger,[1] Nathalie Daniel,[1] Béatrice Mandon-Pépin,[1] Maëlle Pannetier,[1] and Eric Pailhoux[1]

[1]Université Paris-Saclay, INRAE, ENVA, UVSQ, BREED, 78350, Jouy-en-Josas, France; and [2]AP-HP, Pôle biologie-Pathologie Henri Mondor, Créteil, France; INSERM IMRB U955, Créteil, France

ORCiD number: 0000-0002-2705-7723 (G. Jolivet).

Abbreviations: AMH, anti-Müllerian hormone; dpc, days post coitum; dpp, days postpartum; GC/MS, gas chromatography/mass spectrometry; HES, hematoxylin–eosin–saffron; ISH, in situ hybridization; KO, knockout; qPCR, quantitative polymerase chain reaction; SRY, Sex-determining Region of Y chromosome; WT, wild type

Received: 17 March 2021; Editorial Decision: 29 September 2021; First Published Online: 6 October 2021; Corrected and Typeset: 12 November 2021.

Abstract

AROMATASE is encoded by the *CYP19A1* gene and is the cytochrome enzyme responsible for estrogen synthesis in vertebrates. In most mammals, a peak of *CYP19A1* gene expression occurs in the fetal XX gonad when sexual differentiation is initiated. To elucidate the role of this peak, we produced 3 lines of TALEN genetically edited *CYP19A1* knockout (KO) rabbits that were devoid of any estradiol production. All the KO XX rabbits developed as females with aberrantly small ovaries in adulthood, an almost empty reserve of primordial follicles, and very few large antrum follicles. Ovulation never occurred. Our histological, immunohistological, and transcriptomic analyses showed that the estradiol surge in the XX fetal rabbit gonad is not essential to its determination as an ovary, or for meiosis. However, it is mandatory for the high proliferation and differentiation of both somatic and germ cells, and consequently for establishment of the ovarian reserve.

Key Words: CYP19A1, AROMATASE, sex determination, ovary, rabbit, TALEN

Gonad differentiation is a key step of sex determination. In mammals, it is triggered by SRY (Sex-determining Region of Y chromosome), which acts as the master testis-determining factor by upregulating SOX9 in the undifferentiated XY gonad (1, 2). In an XX context, the gonads differentiate into ovaries through activation of the canonical β-catenin pathway enhanced by 2 secreted proteins, RSPO1 and WNT4 (3-5). As well as the β-catenin pathway, the *FOXL2* gene has also been shown to be critical for ovarian differentiation in a nonrodent mammalian species,

ISSN Online 1945-7170

the goat (6). Among other functions, the FOXL2 transcription factor controls estrogen synthesis in early developing goat ovaries by upregulating the *CYP19A1* gene that encodes AROMATASE (7, 8), the latter being the only enzyme responsible for estrogen synthesis in vertebrates. Following *FOXL2* loss of function in goats, undifferentiated gonads stop expressing *CYP19A1*, upregulate *SOX9*, and differentiate as testes (6). One remaining question concerns the role of *CYP19A1* and estrogens in ovarian differentiation and in the female-to-male sex reversal process that occurs in *FOXL2* KO (knockout) gonads.

AROMATASE specifically converts 3 androgenic substrates (androstenedione, testosterone, and 17alpha-testosterone) to estrone, estradiol, and estriol, respectively. AROMATASE is the product of the *CYP19A1* gene, which is the only member of its gene family. Although *CYP19A1* is generally considered to be mainly expressed by gonads in adults, its physiologically significant expression has been reported in numerous tissues or organs such as bones, adipose tissue, brain, or placenta (expression in the last one depending on the species; for a review see (9) and references therein).

In mammals, expression of the *CYP19A1* gene starts early, at around implantation in the embryo in rabbits (10, 11), pigs, and ruminants (12). A second burst of expression has been reported later in fetal life in the ovaries, but not in testes, shortly after the sex determination process. This was described in rabbits (11, 13-15), sheep (16-18), goats (19), bovines (20-22), and humans (23) by RNA measurements or estrogen assays in gonads or gonadal culture media. This peak is transitory and lasts until meiosis is initiated. *CYP19A1* gene expression subsequently increases gradually in line with follicle differentiation. It culminates in antrum follicles, where mural granulosa cells are the site of expression. In the past, efforts were made to determine the physiological significance of this fetal peak of expression in the rabbit species; George et al. (14) suggested that the local production of estrogens in the XX gonad was a key event for initiation of the differentiation of the female fetal gonad, but this hypothesis has still not been proven. In birds (24, 25) and fish (26), it has been shown that estrogens are major determinants of the ovarian orientation of undifferentiated gonads in fetal or larval life. We therefore decided to investigate the role of the fetal peak of estrogen in the mammalian gonad, and more specifically whether it is mandatory for ovary differentiation in mammals.

To achieve this, we decided to suppress the expression of the *CYP19A1* gene in a mammal other than the mouse. Indeed, rodents represent some of the few mammalian species without a detectable peak of expression at this developmental stage in the fetal XX gonad, in other words, before meiosis. Thanks to the TALEN methodology that has already been shown to be efficient for gene targeting in the rabbit (27, 28), we produced *CYP19A1* KO rabbits completely devoid of estrogen secretion. We report here on the phenotype of all XX *CYP19A1* KO ($ARO^{-/-}$) female rabbits with severe ovarian developmental defects. A series of histological and genetic analyses was thus performed from the early stages of gonadal differentiation in order to investigate the mechanisms involved.

Materials and Methods

Animals

New Zealand rabbits (NZ1777, Hypharm, Rousssay, France) were bred at the SAAJ rabbit facility (Jouy-en-Josas, France). All experiments were performed with the approval of the French Ministry MENESR (accreditation number APAFIS#6775-2016091911407980 vI) and in accordance with the guidelines issued by the local committee for ethics in animal experimentation (COMETHEA, Jouy-en-Josas). All scientists working directly with the animals possessed an animal experimentation license delivered by the French veterinary services. Hormonal treatments for superovulation and surgical procedures for embryo transfer were all performed as previously described (28).

Design of TALEN Sequences and Plasmid Constructs

Exon II of the rabbit AROMATASE gene was targeted to create InDel mutations near the site of initiation of translation (ATG site). The target sequences (left arm: 5′-TGCTTCATCTGAAGCCA-3′ (sense); right arm: 5′-TGGGTTCAGTATTTCCA-3′ (antisense); 16 bases spaced) were chosen using ZiFiT Targeter software (http://zifit.partners.org). No homology was identified at any other location in the rabbit genome that might represent a potential off-target site (Table 1 (29)). The TALEN were constructed as described elsewhere (30) (see Supplementary Methods (29)). Each TALEN RNA was diluted (100 ng/µL) in injection buffer (Millipore, France) and stored at –80°C until use.

Generation of Mutant Rabbits

Embryos produced from superovulated females were injected at the single-cell stage with an equimolar mixture of left and right arm TALEN mRNAs (50 ng/µL each). These injected embryos were then implanted 3 to 4 hours after injection into the oviducts of anesthetized recipient rabbits via laparotomy. Details concerning the handling of females and embryos have been described elsewhere (28).

Offspring were screened for the presence of InDel mutations using genomic DNA extracted from ear clips (31). Founders were detected and mutations characterized using 1 set of primers located far upstream and downstream of the targeted ATG (F0/R0, Fig. 1 and Table 2 for all primer sequences (29)). The amplified fragments were sequenced (Eurofins Genomics, Courtaboeuf, France) and the extent of the mutation was deduced by comparing it with the sequence of a wild-type (WT) rabbit.

For the further routine screening of mutants, quantitative polymerase chain reaction (qPCR) (Fast SYBR Green Master Mix, Applied Biosystems, ThermoFisher, France) was performed using 2 sets of primers: *CYP19A1* gene specific primers flanking the position of the characterized InDel mutations (F1/R1, Table 2 (29)) and another set to amplify a 2-copy reference gene (rabbit *beta GLOBIN* gene, ENSOCUG00000000568). Using the Δ(ΔCt) method with a WT rabbit DNA as the reference, we deduced the copy number of the *CYP19A1* allele in each DNA sample (no amplification = the 2 alleles are mutant [$ARO^{-/-}$ genotype]; 1 copy = 1 mutant allele [$ARO^{-/+}$ genotype]; 2 copies = WT or $ARO^{+/+}$ genotype).

The presence/absence of the Y chromosome was deduced from amplification of the *SRY* gene through PCR analyses with the rabbit *beta GLOBIN* gene as the positive control for PCR and *SRY* specific primers (Table 2 (29)). All rabbits were tested to determine their genomic sex in parallel with external and histological observations. In the present paper, mentions of the XY or XX genotype always refer to the PCR determination.

Histological and Immunohistological Analyses

Immediately after sampling, gonads were immersed in Bouin's fixative or paraformaldehyde (4% PAF in phosphate-buffered saline 1×), fixed for 24 to 72 hours and then paraffin embedded. Microtome sections 5 µm thick were processed. Hematoxylin–eosin–saffron (HES) staining was performed by the @Bridge platform (INRAE, Jouy-en-Josas) using an automatic Varistain Slide Stainer (Thermo Fisher Scientific). Sirius Red-Fast Green staining was performed manually.

In situ hybridization (ISH) was performed using the RNAscope ISH methodology (ACD, Bio-Techne SAS, Rennes, France). Briefly, probes around 1000 nt long were designed and produced by the manufacturer in order to match the full-length cDNA of interest, taking care to reduce any cross-hybridization with nonspecific targets. The list of all synthesized probes is given in Table 3 (29). Hybridization was performed on 5-µm sections from PAF-fixed tissue using labeling kits (RNAscope 2.5HD assay-brown or -red, or RNAscope 2.5HD duplex chromogenic assay blue [conjugated to horse radish peroxidase] and red [conjugated to alkaline phosphatase]) as recommended by the manufacturer. Red labeling (Fast Red) was observed as visible or fluorescent signals. Hybridization was considered to be positive when at least 1 dot was observed in a cell.

Immunohistological analyses were performed on 5-µm sections from PAF-fixed tissue. Table 4 (29) summarizes the antibodies used.

All stained sections (visible or fluorescent) were scanned using a 3DHISTECH panoramic scanner at the @Bridge platform (INRAE, Jouy-en-Josas).

When necessary, the density of positive cells (immunohistology or ISH) was determined. An area was delimited manually, the surface was calculated automatically (CaseViewer, 3DHISTECH Ltd) and the cells counted manually. Density was calculated from the ratio between the number of cells and the surface of the delimited area. Values are given as arbitrary units to enable comparisons between different genotypes.

RNA Extraction and Reverse Transcription-qPCR Analyses

RNA extraction and reverse transcription (RT)-qPCR analyses were performed as described elsewhere (13). Gonads from rabbit fetuses were collected and frozen immediately at –80°C. Total RNA from each gonad was extracted using the RNeasy® MicroKit (Qiagen, France). Quantitative PCR was performed on reverse transcribed RNAs (High Capacity Reverse cDNA Transcription kit and its set of random primers; Applied Biosystems, ThermoFisher, France).

Quantification was achieved with the SYBR Green quantitative PCR kit (Applied Biosystems) with dilutions of the RT reactions and sets of primers designed using Primer Express software (Applied Biosystem). Whenever possible, qPCR primers were chosen on separate exons in order to avoid DNA amplification, and all amplicons were 100 base pairs long. Several PCR sets of primers were those published previously (13). Other sets of primers are shown in Table 2 (29). Analyses were performed using the Δ(ΔCt) method (Biogazelle QBasePlus software, Biogazelle NV, Ghent, Belgium) and the normalizing genes previously selected (*H2AFx*, *HPRT*, *YwHaz* (13)). Care was taken to consider Ct values within the linear amplification zone. Gene expression was considered to be significant when the Ct values obtained using 2-5 ng of cDNA in each q-PCR reaction were lower than 34, and when a single DNA fragment with the expected size was amplified in each q-PCR reaction. For each series of samples (ie, each graph), data were normalized to 1 calibrator to correct for inter-run variations. Finally, each graph presents mRNA fold changes relative to the lowest data of the series.

Measurement of Estradiol, Testosterone, and Anti-Mülllerian Hormone Levels in Serum Samples and Fetal Gonads

Estradiol and testosterone were assayed by gas chromatography/mass spectrometry (GC/MS) according to the protocol described by Giton et al. (32), with some modifications (33). Female $ARO^{-/-}$ rabbit serum was used as the matrix for calibrators and quality control standards after 2 charcoal dextran treatments. Sample extraction and purification, and the derivatization and determination of estradiol and testosterone levels in serum samples and fetal gonads are described in detail elsewhere (29). Anti-Müllerian hormone levels (AMH) were determined in 50-µL aliquots of serum using an enzyme-linked immunosorbent assay kit (AMH GenII ELISA, with AMH Gen II calibrators and controls, Beckman Coulter, Villepinte, France) as previously described (34).

Statistics

Statistical analyses were performed using GraphPad Prism 7 software (GraphPad Software Inc., La Jolla, CA, USA). Because of the small number of samples in each group, comparisons between values were made using the Mann–Whitney test for nonparametric values. A probability lower than .05 was required to achieve statistical significance.

Results

Generation of 3 Aromatase Mutant Rabbit Lines Producing no Estradiol

The TALEN subunits were designed to generate *InDel* mutations through nonhomologous end joining near the initiation site of translation of the *CYP19A1* gene as described in Fig. 1. After transferring 67 injected embryos to 3 recipient female rabbits, 6 founders (2 males and 4 females) harboring mutant alleles were characterized from 11 neonates. Each founder (F0) was mated with a WT counterpart in order to transmit a mutant allele to the descendants and generate mutant lines carrying 1 mutated allele per line.

Three mutant lines, each harboring a specific mutant allele, were generated and studied. Homozygous ($ARO^{-/-}$) rabbits were generated by crossing heterozygous XX and XY $ARO^{+/-}$ rabbits, or by crossing XY $ARO^{-/-}$ and XX $AR+^{-/-}$ rabbits (all XY rabbits $ARO^{+/-}$ and $ARO^{-/-}$ were able to get litters and transmit the mutation). Mating was performed between rabbits within each line in order to avoid mixing the various mutant alleles.

The mutations are shown in Fig. 1. A 339, 498, or 829 nt long deletion was observed in each of the alleles, named Δ339, Δ498, and Δ829, respectively. Briefly, the mutations eliminated the translation initiation site (ATG codon), so no protein was expected to be translated from any of these mutant alleles. Otherwise, the deletions should in theory lead to the elimination of 48 amino acids in the N-terminus of the AROMATASE enzyme. As previously published (35), these amino acids encompass the signal anchor responsible for translocation of the protein to the endoplasmic reticulum. It is therefore expected that if a protein is translated from the mutant mRNAs, it has a good chance of not being properly integrated into the endoplasmic reticulum bilayer, and therefore of being nonfunctional.

Finally, to confirm the absence of any active AROMATASE enzyme, we searched for estradiol using GC/MS on rabbit serum samples collected after birth and in fetal gonads. Estradiol levels in sera from $ARO^{-/-}$ XX females after birth were below the limit of quantification (LOQ = 0.2 pg/mL) whatever the age of the animals, while in WT ($ARO^{+/+}$) and heterozygous ($ARO^{+/-}$) females these levels rose gradually in line with the age of the animal (Fig. 2). Estradiol concentrations were much lower in WT males than in females. Testosterone levels were similar in sera from all XX rabbits ($ARO^{-/-}$, WT, or $ARO^{+/-}$), but always much lower than in males.

GC/MS was also used to determine the steroid content of the gonads in fetuses aged 28 days post coitum (dpc). The estradiol content was undetectable in gonads from all $ARO^{-/-}$ XX fetuses and in all XY gonads, but it was always detected (even sometimes at very low levels) in XX gonads from $ARO^{+/-}$ and WT genotypes (Fig. 2). Testosterone was not detected in any XX gonads, whatever their genotype. This shows that androgens were not oversynthesized or accumulated in XX $ARO^{-/-}$ gonads. Finally, these data also showed that neither estradiol nor testosterone of maternal or placental origin was detected in 28 dpc fetal gonads.

XX $ARO^{+/-}$ Rabbits Were Fertile, With Normal Genital Tracts and Normal Gonad Morphology

In the 3 mutant lines, XX $ARO^{+/-}$ rabbits were viable until adulthood and did not apparently suffer from any metabolic or postural diseases until they were at least 2 years old. No modifications to their external genitalia were visible. All were fertile and gave birth to progeny. Their sexual behavior was not studied. The number of neonates per litter from heterozygous mating (♀$ARO^{+/-}$ × ♂$ARO^{+/-}$) was similar to that of WT mating (♀WT × ♂WT) (Supplementary Figure 1 (29)). The percentages of mating without pregnancy did not differ: 37.9% (11 null/29) in WT × WT animals vs 35.3% (23 null/65) in heterozygous × heterozygous animals. All this suggests that the fertility of heterozygous animals was not affected.

At puberty (5-6 months after birth), the size and overall morphology of genital tracts and gonads did not differ

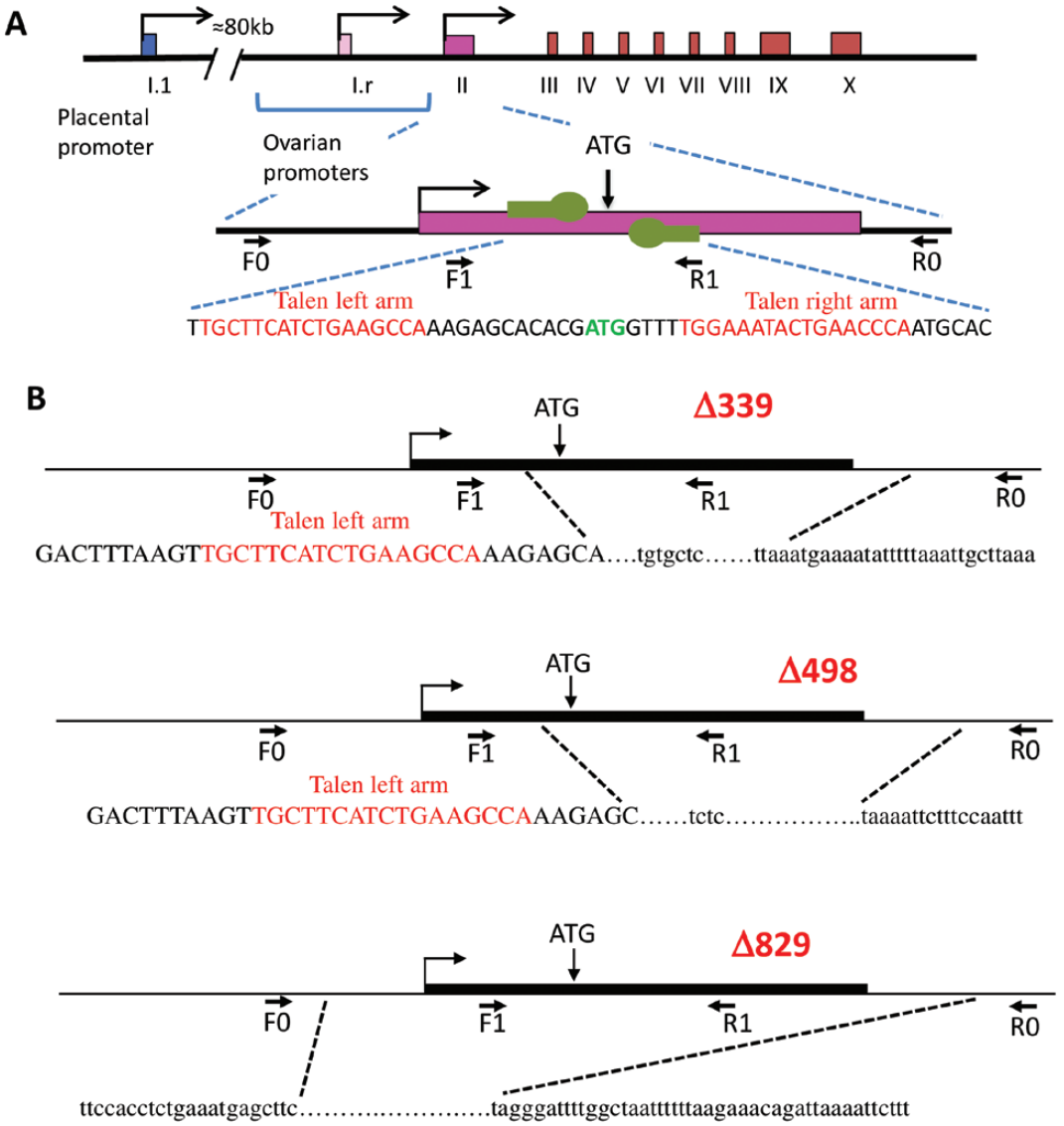

Figure 1. TALEN induced indel mutations in the rabbit *CYP19A1* gene. (A) Structure of the rabbit aromatase gene, with already described tissue specific promoters (69), ie, the I.1 placental promoter at around 80 kb upstream of the transcription start point (tsp, marked by squared arrows) and the 2 proximal ovarian promoters I.r and II. The enlargement shows the sequence of exon II with the initiation site of translation (ATG in green letters). The 2 subunits (left and right arms) of the TALEN are shown as green symbols and the targeted sequence is written in red. The horizontal black arrows indicate the primers used for the PCR detection of mutants in founders (F0/R0 set) and for routine qPCR genotyping (F1/R1 set). (B) Sequences of mutant alleles: Δ339, Δ498, and Δ829. Capital letters refer to the exon sequence and lowercase letters to the intron sequence. The deletion spans 339 nucleotides (nt) in the Δ339 mutant allele (149 nt at the 3′ end of exon II and 190 nt of intron 2) and 498 nt in the Δ498 mutant allele (148 nt at the 3′ end of exon II and 350 nt of intron 2), both with the insertion of a few nucleotides at the repair position. In the Δ829 allele, the mutation consisted in the elimination of 829 nt encompassing 250 nt upstream of the start of exon II (transcription start site of the gene as regards the ovarian promoter), the totality of the second exon (263 nt) and 316 nt in the second intron. All mutations suppressed the ATG codon and the splice donor site at the 3′ extremity of exon II.

between heterozygous and WT XX rabbits (Supplementary Figure 2 (29)). Because all the measured parameters did not differ between heterozygous and WT females (similar estradiol and testosterone serum levels, similar prolificacy, similar overall structure of the genital tracts and ovaries), we used ovary samples indifferently from WT or heterozygous females as references. Nevertheless, in our paper, the genotype (WT or heterozygous) is always reported in the legends of all figures.

XX *ARO*$^{-/-}$ Rabbits Developed Small Female Genital Tracts, Ovaries With Almost no Follicular Reserve and Very Few Antral Follicles

All XX *ARO*$^{-/-}$ rabbits were viable and free of any metabolic or postural disease at least until 1.5 years after birth. No apparent modifications to their external genitalia were visible. The sexual behavior of XX *ARO*$^{-/-}$ rabbits was not studied.

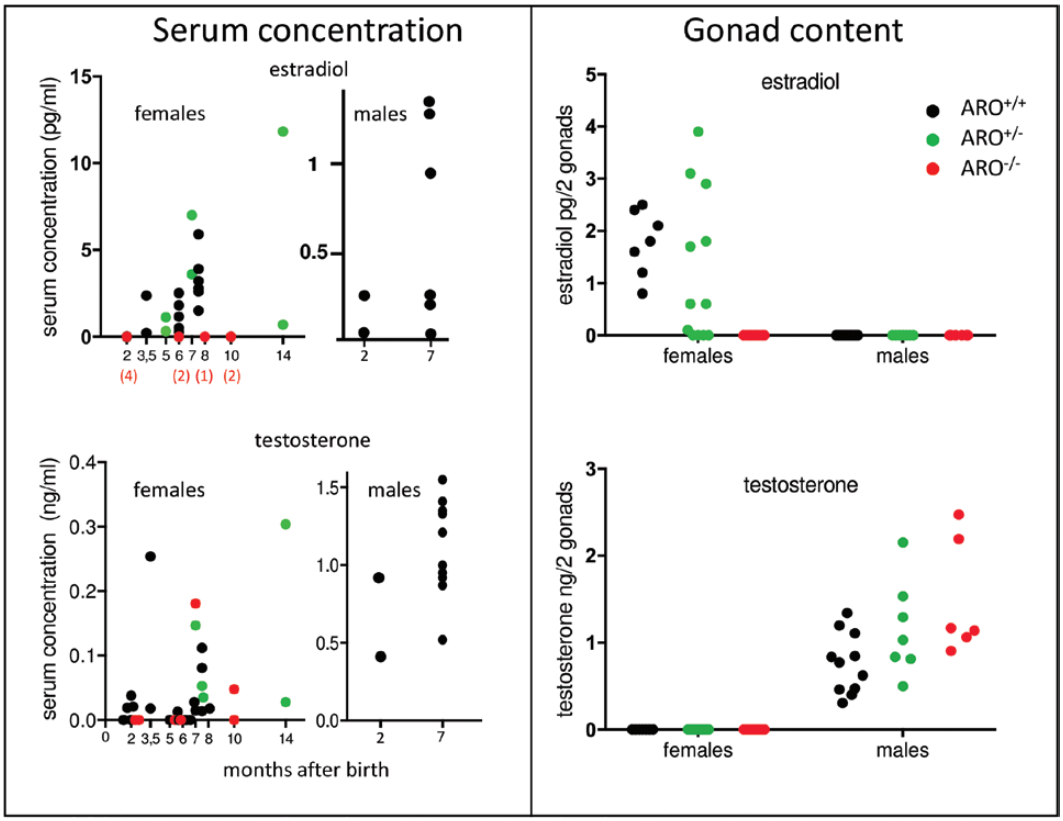

Figure 2. Estradiol and testosterone in serum from female rabbits and in gonads from fetuses. Serum samples were collected from 2 to 14 months after birth. Fetal gonads were collected 28 days after mating. Pairs of gonads were immediately frozen at –80°C. Steroid concentrations were measured by GC/MS in wild-type XX rabbits (black points), *ARO*$^{+/-}$ rabbits (green points) and *ARO*$^{-/-}$ rabbits (red points). The number of serum samples analyzed from *ARO*$^{-/-}$ females is shown in brackets in red. Note the difference of scale between male and female serum levels. Gonad contents were assayed in the pool of both gonads from 1 animal. The same samples were used to assay testosterone and estradiol.

Obvious modifications of the genital tracts and ovaries could be seen in XX *ARO*$^{-/-}$ rabbits from the 3 lines with similar characteristics. After puberty, a typical phenotype was observed, with underdeveloped uterine horns, oviducts, and pavilions. Their size was clearly smaller than in WT or heterozygous females (Supplementary Figure 2 (29)). In all 3 lines, XX *ARO*$^{-/-}$ gonads developed as ovaries (Fig. 3 and Supplementary Figure 3 (29)) but with a very small size. In spite of individual variations possibly due to the genetic heterogeneity of our rabbits, a major phenotype affecting the differentiation of ovaries was observed similarly in the 3 lines whatever the extent of gene deletion. Since this phenotype was shared by the 3 lines, it was hardly attributable to any off-target genomic alterations, but was very probably linked to the *CYP19A1* gene deletion.

The ovaries contained almost no primordial follicles and few primary and secondary follicles, and were filled with numerous remnants of atretic follicles. The abundant follicle reserve composed of primordial follicles and observed at the cortex of WT ovaries (Fig. 3A and 3B) was absent from *ARO*$^{-/-}$ mutant gonads (Fig. 3C-3E). Nevertheless, some follicles developed to reach the large antrum stage in *ARO*$^{-/-}$ ovaries, displaying granulosa and theca cell layers, oocyte and cumulus. The number of large antrum follicles was high in some females (see the ovary of the Δ829 female in Supplementary Figure 3 (29)), possibly reflecting the gonadotropin surge that occurs at early puberty (around 5-6 months in the rabbit). Numerous Call-Exner bodies (spherical deposits of basal lamina matrix surrounded by granulosa cells, observed in rabbits and some other mammals) were observed in the granulosa of growing follicles in *ARO*$^{-/-}$ ovaries, as classically observed in WT animals (36). The number of pyknotic cells or cells with densely stained nuclei was small.

The expression of *RSPO2* and *FOXL2* marker genes, specific to the oocyte and granulosa cells, respectively, in differentiating follicles, was studied by in situ hybridization (ISH, Fig. 4). In the *ARO*$^{-/-}$ ovary, the rare oocytes detected were positive for *RSPO2* labeling (Fig. 4A), and granulosa cells were positive for *FOXL2* (Fig. 4B). In WT ovaries, AROMATASE was immunodetected in a small number of follicles with an antrum, thus characterizing pre-ovulatory follicles (Fig. 4C). AMH was immunodetected in the granulosa cells of numerous follicles in WT ovaries, except

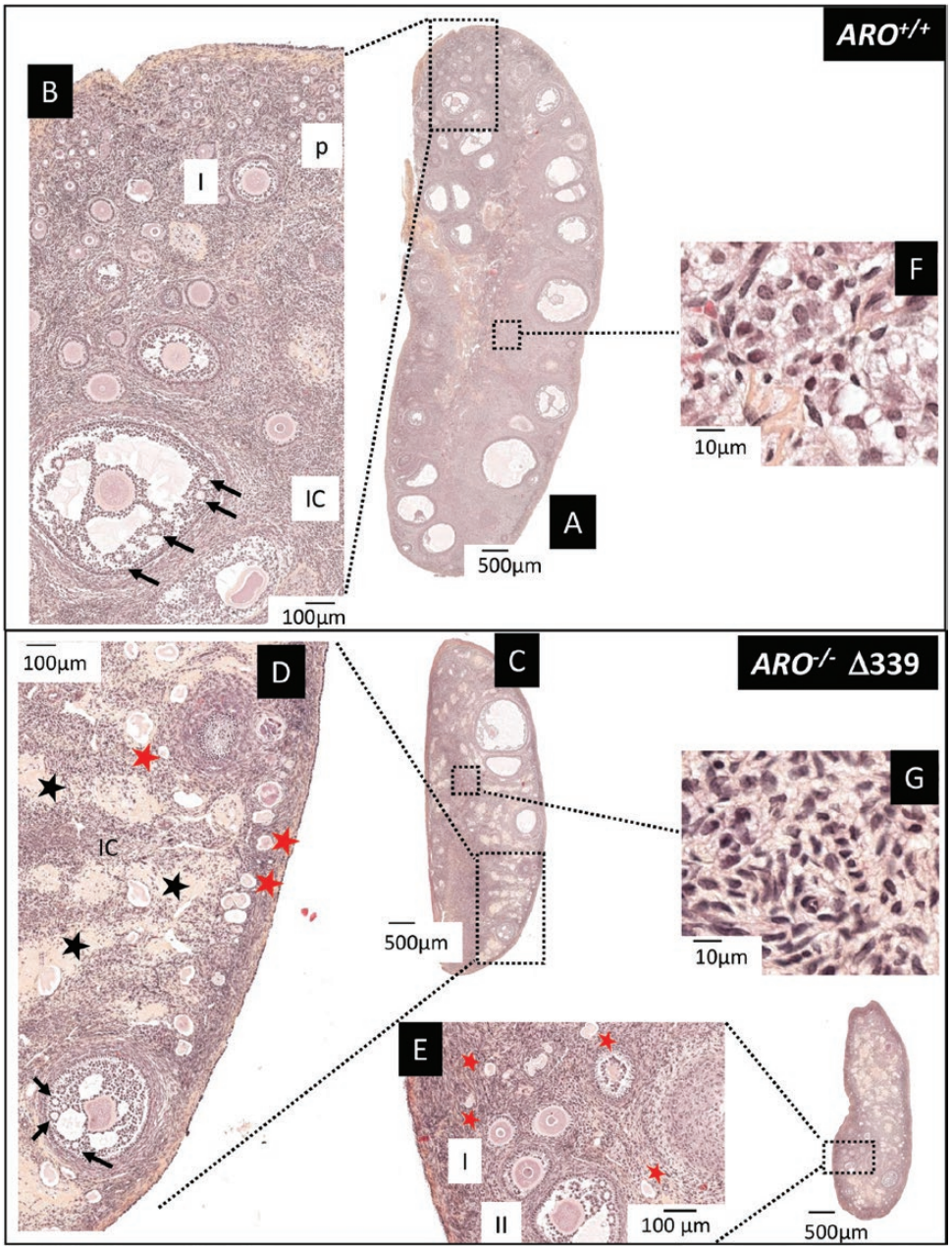

Figure 3. Ovaries from adult *ARO*$^{-/-}$ rabbits were small with few follicles and filled with collagen-rich connective tissue. Ovaries from wild-type female rabbits (*ARO*$^{+/+}$, A and B) and from the mutant *ARO*$^{-/-}$ line Δ339 (C and D) were fixed in PAF then HES-stained. The females were 5.5 months old. Two distinct sections of the same ovary are shown for the *ARO*$^{-/-}$ mutant in order to reveal follicles that were otherwise not visible. Enlarged zones highlight the different types of follicles. Black arrows = Call–Exner bodies. Black stars = accumulation of fibrous tissue. Red stars = remnants of degenerated follicles. "p" = primordial follicle; I = primary follicle; II = secondary follicle; IC = interstitial cells. The phenotype of the *ARO*$^{-/-}$ ovary was similar in the other lines, Δ498 and Δ829 (Supplementary Figure 3 (29)).

those positive for AROMATASE. In *ARO*$^{-/-}$ ovaries, the granulosa cells of all follicles were AROMATASE negative and AMH positive (Fig. 4D and Supplementary Figure 4 (29)). However, serum AMH levels were lower in *ARO*$^{-/-}$ females, reflecting the small number of follicles and/or their poor capacity for synthesis.

The DMRT1 and SOX9 factors previously reported in mice as transcription factors involved in maintaining adult male testis identity (see (2) and references therein), were searched for using immunodetection (Fig. 5). In ARO$^{-/-}$ rabbits, 5 to 6 months after birth, granulosa cells in some follicles were positive for DMRT1, while few DMRT1-positive cells were detected in WT ovaries. No significant staining was observed when using the SOX9 antibody on adult ovary sections whatever the genotype.

Intense modifications affected the medulla of the ovary. In WT rabbits, the medulla mostly consisted in interstitial tissue composed of cells with a large clear cytoplasm

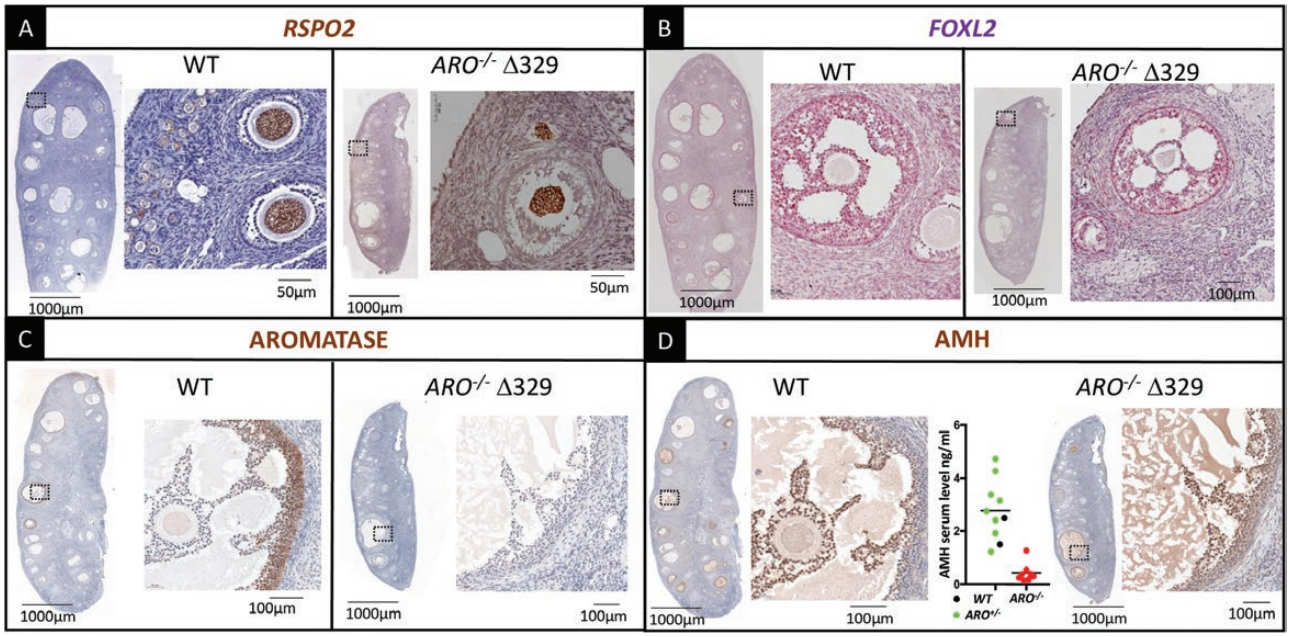

Figure 4. *RSPO2*, *FOXL2*, and AMH were detected in wild-type (WT)and ARO$^{-/-}$ adult ovaries. In situ hybridization to localize the mRNA of *RSPO2* and *FOXL2* genes and for the immunodetection of AROMATASE and AMH in adult ovaries. Ovaries were collected from WT or *ARO*$^{-/-}$ Δ329 females aged 5-6 months. The expression of *RSPO2* (A) and *FOXL2* (B) genes was detected using ISH probes. AROMATASE (C) and AMH (D) were detected by immunohistochemistry on 2 adjacent sections. The *RSPO2* and *FOXL2* probes respectively labeled the cytoplasm of oocytes (brown dots) and of granulosa cells (red dots) from all follicles, from the primordial to the antrum stages in both WT and *ARO–/–* rabbits. Some thecal cells were also positive for *FOXL2* labeling in both genotypes. Mural granulosa cells from pre-ovulatory follicles were positively labeled by the anti-AROMATASE antibody in WT ovaries (brown colored); no cells were positive in *ARO*$^{-/-}$ ovaries. The anti-AMH antibody labeled most granulosa cells of growing follicles in WT ovaries (brown colored), except those positive for AROMATASE. In *ARO*$^{-/-}$ ovaries, all follicles with antrum were positively labeled. Similar staining was observed in females from the other 2 strains (Supplementary Figure 4 (29)). The graph represents AMH serum levels in *WT* (black points), *ARO*$^{+/-}$ (green points) and *ARO*$^{-/-}$ (red points) females.

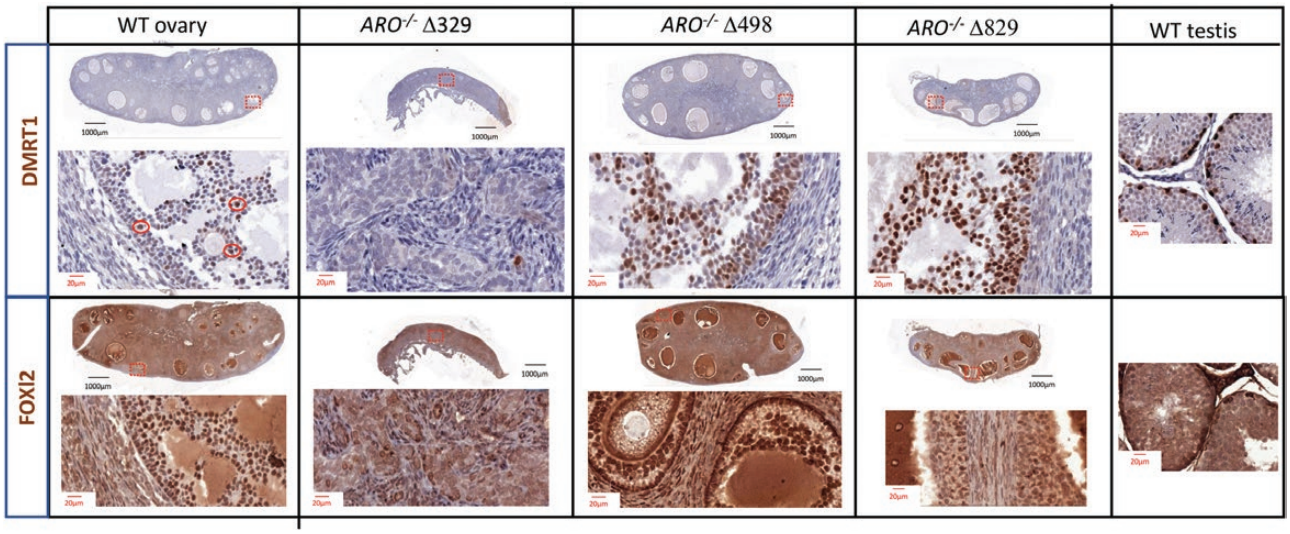

Figure 5. DMRT1 and FOXL2 immunodetection in wild-type (WT) and ARO$^{-/-}$ ovaries. Ovaries were collected from WT or *ARO*$^{-/-}$ Δ339, Δ498, and Δ829 females aged 5-6 months. Immunolabeling was performed simultaneously on adult testis as a positive control in order to detect DMRT1- and SOX9-positive cells in seminiferous tubes. Granulosa cells from a small number of large antrum follicles were positively labeled by the anti-DMRT1 antibody in *ARO*$^{-/-}$ ovaries in lines Δ498 and Δ829 but not in Δ339, simply because of the lack of large antrum follicles; few cells were DMRT1-positive in WT ovaries.

and rounded, regular-shaped nucleus (Fig. 3F); besides, in *ARO*$^{-/-}$ ovaries, the interstitial tissue appeared as a mixture of cells of heterogeneous shape with angular nuclei (Fig. 3G). Several areas were detected as being filled with fibrous material that was rich in collagen and devoid of cells (Fig. 3 and Supplementary Figure 3 (29)).

Some of the heterozygous ($ARO^{+/-}$) and homozygous ($ARO^{-/-}$) 10 month old XX rabbits were treated with hormones to induce ovulation, then mated and sacrificed to collect their gonads for histological analysis. Ovulation rupture points were observed in ovaries from $ARO^{+/-}$ rabbits, but not in $ARO^{-/-}$ ovaries (Supplementary Figure 5 (29)). While several primordial, primary, pre-antral, and antral follicles were detected at the cortical periphery of ovaries from $ARO^{+/-}$ rabbits after superovulation treatment, no primordial and very few primary follicles were seen in the treated $ARO^{-/-}$ ovarian cortex. Some large antrum type follicles were observed in $ARO^{-/-}$ ovaries, with developed granulosa, theca cells and oocytes.

The Mutation Impacted XX Gonads From the Early Stages of Their Differentiation

Our goal was to determine when and how ovaries were impacted by the lack of functional AROMATASE enzyme and estradiol during fetal life. Pregnancy spans a period of 31 days in the rabbit species. The transition from an indeterminate gonad to an ovary or testis occurs at around 16 to 18 dpc. The peak of *CYP19A1* gene expression starts at 18 dpc in the ovary, concomitantly with an increase in the expression of *FOXL2*, *ESR1*, *WNT4*, and *RSPO1* genes (Fig. 6 and (13)). The *RSPO1* and *WNT4* genes are major components of β-catenin signaling which has already been reported as mandatory for early ovarian differentiation in mice and humans (3, 37, 38). The *ESR1* and *ESR2* genes code for α- and β-estrogen receptors, respectively. The *CYP19A1* and *ESR1* genes were expressed by cells in the surface epithelium and those forming invaginated structures arising from this epithelium (20 dpc; Fig. 6, ISH probe labeling). On the other hand, the *FOXL2* gene was mainly expressed in somatic cells beneath the surface epithelium and those surrounding invaginated structures. Expression of the *ESR2* gene coding for estrogen receptor beta was weak at these stages when compared with the levels determined later at birth (34 dpc). As expected, faint labeling was observed by ISH labeling (Fig. 6).

The present study therefore analyzed the fetal gonads from 18 dpc onwards. The gonads from all XX fetuses, both $ARO^{-/-}$ and $ARO^{+/-}$, were differentiated as ovaries with the same morphology apart from a thinner coelomic epithelium in $ARO^{-/-}$ gonads (Fig. 7A). Regardless of developmental stage, XX $ARO^{-/-}$ gonads displayed no evidence of a testicular appearance (for a comparison, see the 18 dpc testis in Supplementary Figure 6 (29)). Numerous OCT4-positive germ cells were detected in both $ARO^{-/-}$ and $ARO^{+/-}$ gonads (Fig. 7B). Mitotic activity was detected by KI67 immunostaining (Fig. 7C). In both $ARO^{+/-}$ and $ARO^{-/-}$ ovaries, KI67-positive cells were mainly present on the ovarian surface facing the abdominal cavity and in invaginated structures beneath. Interestingly, the KI67-positive ovarian surface appeared to be thinner in KO gonads than in the $ARO^{+/-}$ controls (Fig. 7C).

From 20 dpc onwards, more important alterations appeared gradually in $ARO^{-/-}$ ovaries. The cortex was thinner, composed of a single layer of epithelial cells connected to small, nascent ovigerous cords, unlike the thick cortex observed in $ARO^{+/-}$ ovaries, which was connected to numerous large ovigerous cords (Fig. 8A1 and 8A2). A discontinuous layer of cells with small and dense stained nuclei was observed beneath the surface epithelium, which from 22 dpc (Fig. 8B1) formed loose connective tissue between the thin cortex and the inside of the ovary.

Cells in the surface epithelium expressed the *ESR1* gene in both genotypes (Fig. 8A2 and 8B2). The intensity of ISH *ESR1* labeling varied considerably at the surface of $ARO^{+/-}$ ovaries, as shown in Fig. 8 (compare 8A2, A3, B2, B3, which are different sections from the same gonad). Nevertheless, in all treated sections, clusters of labeled *ESR1* cells connected to the surface epithelium were easily observed. Further, in $ARO^{-/-}$ ovaries, labeled *ESR1* cells were mainly dispersed inside the gonad. Similarly, the *FOXL2* ISH probe labeled evenly dispersed cells inside the $ARO^{-/-}$ gonad, which differed from the strongly *FOXL2*-labeled cell cords of the $ARO^{+/-}$ ovary. Numerous *OCT4*-positive germ cells were found in the surface epithelium, interestingly in close contact with somatic cells expressing the *ESR1* gene (Fig. 8A3, 8A4, 8B3, and 8B4). The hybridization signals were weaker in $ARO^{-/-}$ germ cells, possibly related to a modified pluripotency. Since the size of ovaries was smaller in 20 dpc KO fetuses, it is likely that the total number of germ cells was smaller in KO than in WT ovaries.

KI67-positive cells were detected in both types of ovary at 22 dpc (Fig. 9A). However, while many KI67-positive cell layers were detected in the coelomic epithelium of $ARO^{+/-}$ gonads, only 1 layer was visible in $ARO^{-/-}$ gonads. This could reflect a weaker mitotic activity in the coelomic epithelium in $ARO^{-/-}$ ovaries. The γH2AX-antibody, a marker of DNA double-strand breaks, mostly labeled cells with large round nuclei in both types of ovary, probably germ cells (Fig. 9B). The *STRA8* gene expression (a marker of meiosis commitment) was extremely low (Fig. 10). This reflects an absence of commitment to meiosis. Thus γH2AX labeling very likely indicated DNA double-strand breaks occurring at cell death. The density of γH2AX-positive cells did not appear to differ in $ARO^{+/-}$ and $ARO^{-/-}$ ovaries (Fig. 9).

The expression levels of several key marker genes were determined on total RNAs extracted from the whole gonads (Fig. 10). These levels therefore simultaneously

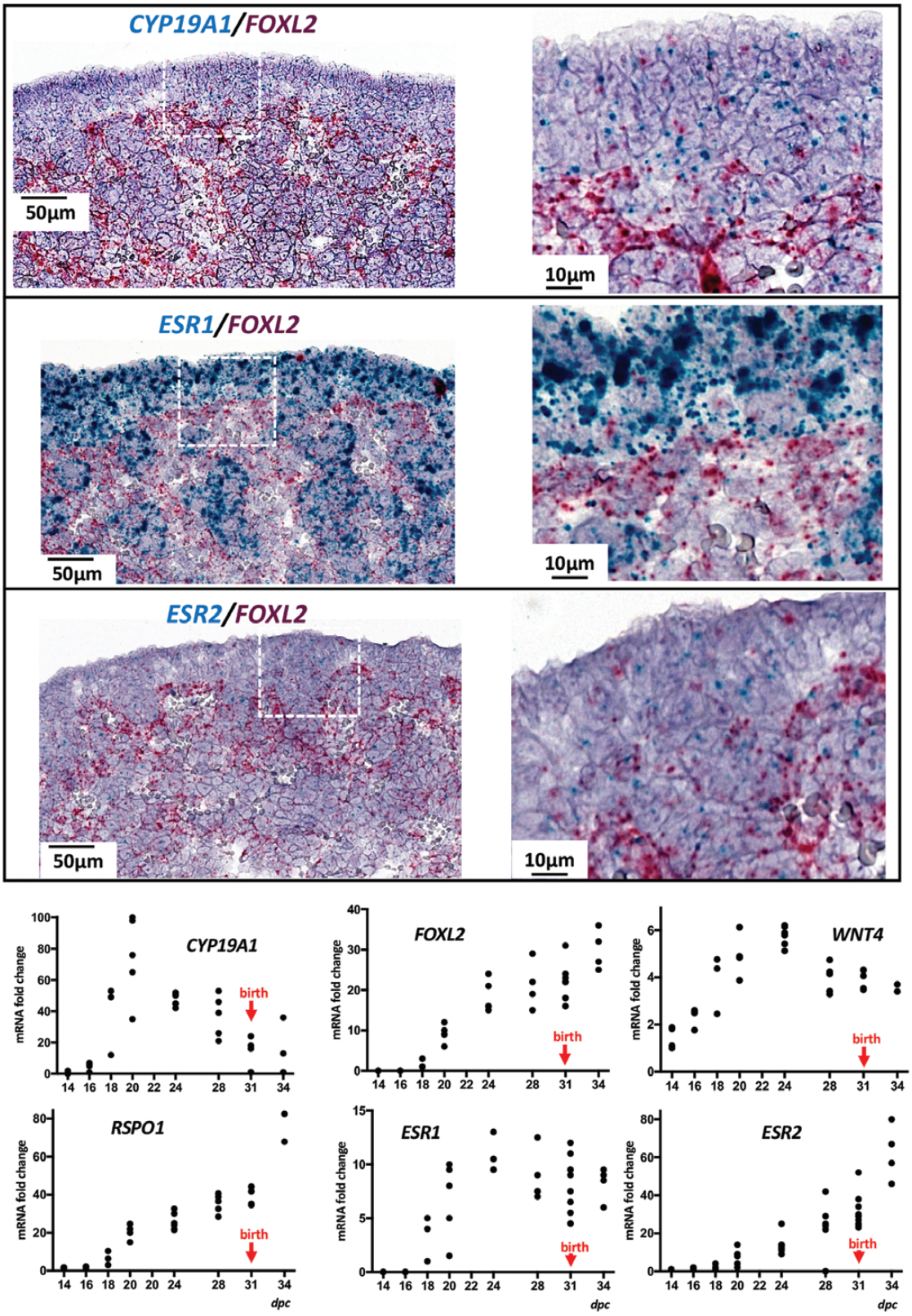

Figure 6. *CYP19A1*, *FOXL2*, *RSPO1*, *WNT4*, and estrogen receptor genes in wild-type 20 dpc fetal ovaries. The cellular localization of gene expression was determined using dual ISH with blue (*CYP19A1*, *ESR1*, *ESR2*) or red (*FOXL2*) labeling. Each image represents the epithelial surface of the ovary and the tissue beneath with an enlargement. Some cells were probably labeled by 2 probes. The diagrams represent mRNA fold changes relative to the lowest point of each graph. Each point represents 1 RNA sample extracted from both gonads of 1 animal at the developmental stage indicated. The same RNA samples are analyzed in the 4 diagrams. The vertical red arrow indicates birth, which occurs 31 days after conception in the rabbit. The *CYP19A1*, *FOXL2*, *RSPO1* and *WNT4* graphs were obtained from data published by Daniel-Carlier et al., 2013 and re analyzed to show fold changes and individual values.

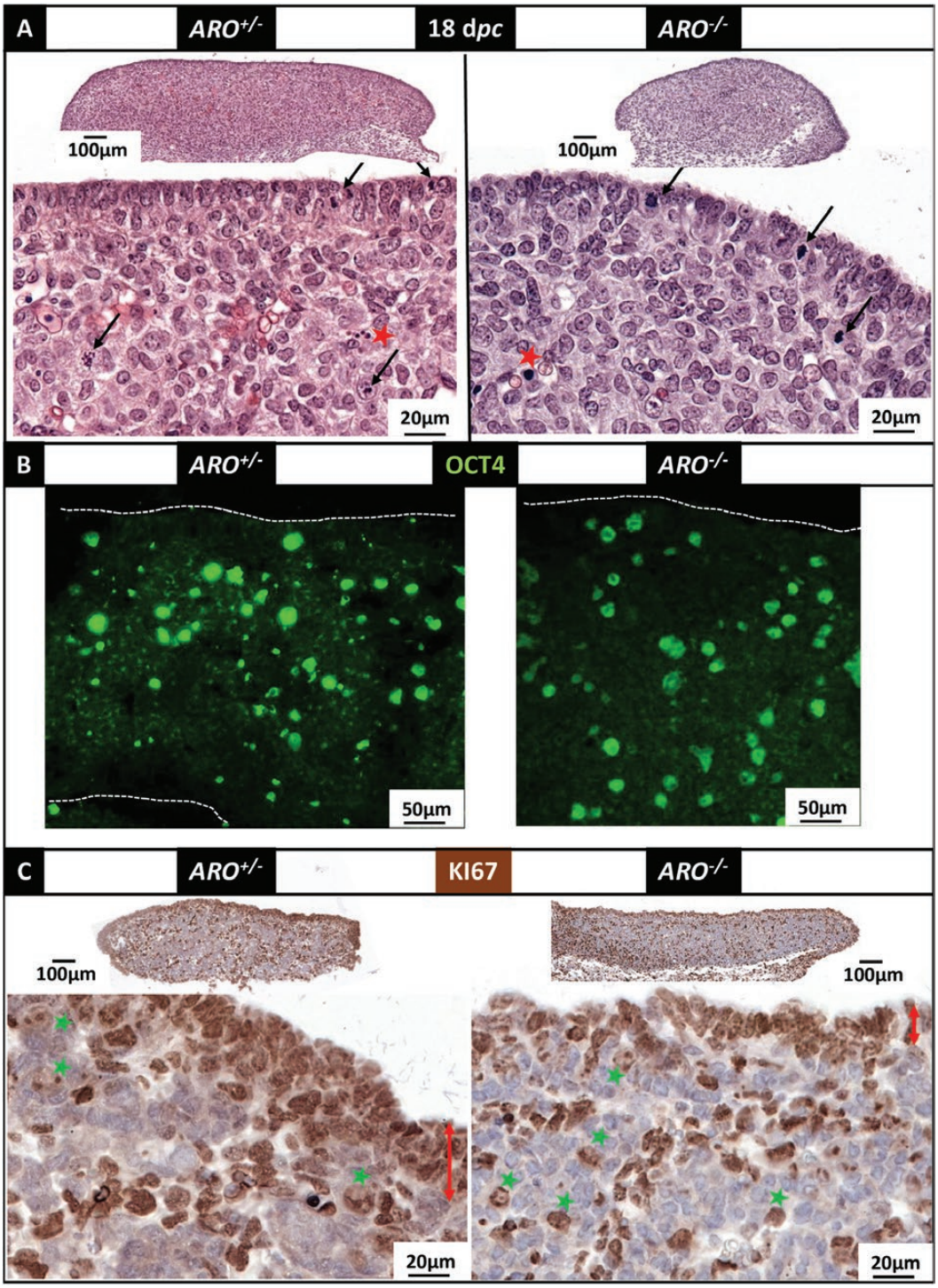

Figure 7. Morphology and detection of OCT4 and KI67 in ovaries from *ARO*$^{+/-}$ and *ARO*$^{-/-}$ 18 dpc old fetuses. Gonads were collected at 18 dpc from *ARO*$^{+/-}$ and *ARO*$^{-/-}$ fetuses, fixed in Bouin's then HES stained (A) or fixed in PAF and then treated for antibody labeling (B and C). (A) HES staining. The surface epithelium appeared as a continuous layer of epithelial cells. Red stars indicate dense nuclei that might correspond to pyknotic nuclei. Arrows indicate figures of mitoses. (B) Detection of OCT4-positive cells. Immune-labeling was visualized using a fluorescent secondary antibody. The nuclei of positive cells (large, round, green-labeled) were dispersed throughout the gonad in both *ARO*$^{+/-}$ and *ARO*$^{-/-}$ ovaries. (C) Detection of KI67-positive cells. Immune labeling was visualized using a peroxidase coupled secondary antibody. Positive cells with brown colored nuclei were found at the surface epithelium, and in rows of cells delimiting cell clusters. The red double arrow indicates the thickness of the surface epithelium enriched with KI67-positive cells. Green stars point to brown light-colored large nuclei, possibly corresponding to germ cells.

reflected the density of expressing cells and their transcriptional activity. The expression of *OCT4*, *FOXL2* and *RSPO1* genes was reduced in *ARO*$^{-/-}$ ovaries, particularly at 22 dpc. The density of OCT4-positive cells was not different in WT and *ARO*$^{-/-}$ ovaries (Fig. 10). This and the quantitative PCR analysis reinforced the hypothesis of a

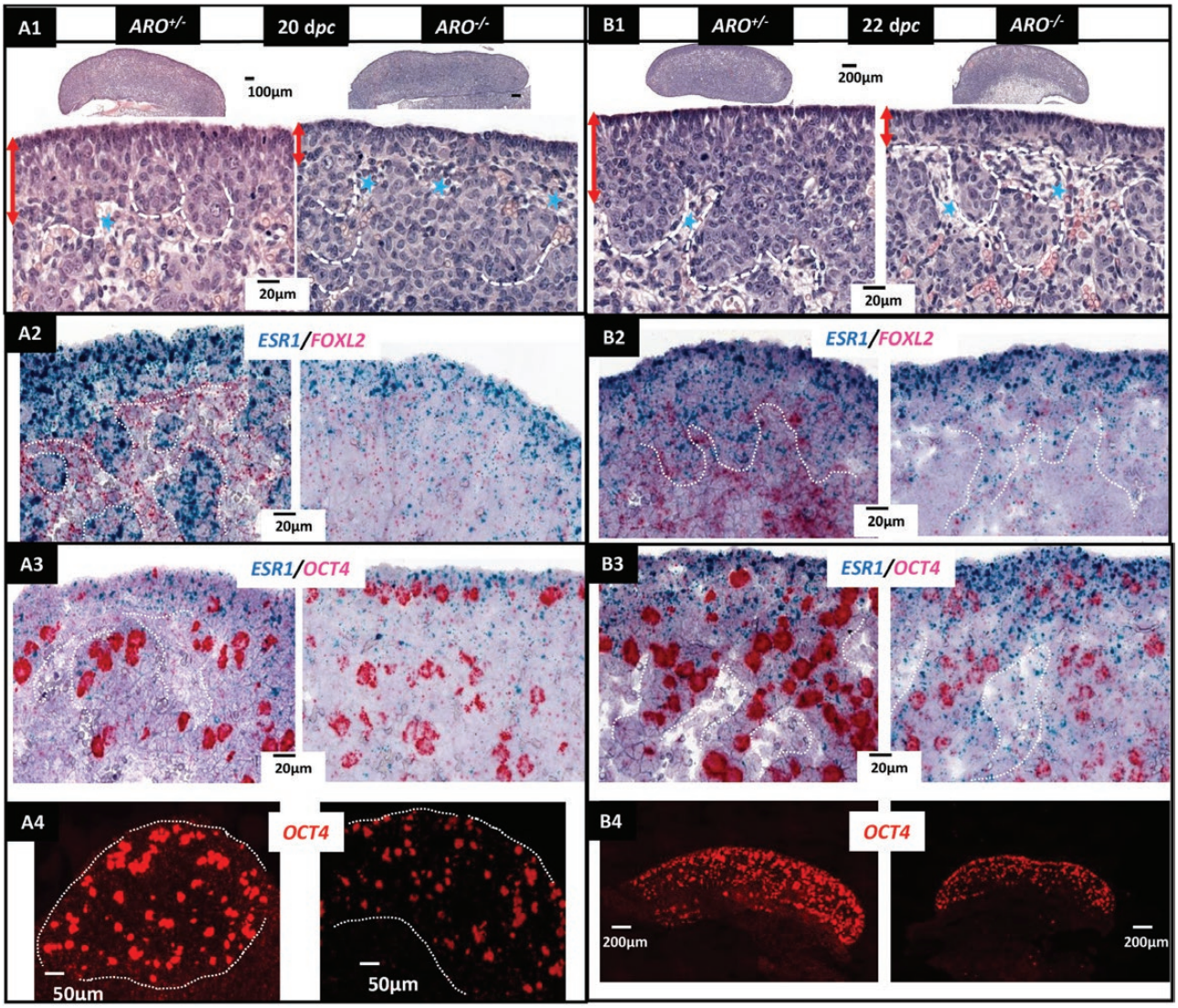

Figure 8. Gradual modifications to *ARO*$^{-/-}$ ovaries at 20 and 22 dpc. Gonads were collected from *ARO*$^{+/-}$ and *ARO*$^{-/-}$ fetuses, fixed in Bouin's then HES stained (A1, B1). Ovigerous nests and cords are highlighted by a dotted white line in A1-3, B1-3. The red double arrow indicates the thickness of the nascent cortex. Blue stars point to connective tissue. In situ hybridization was performed to visualize simultaneously 2 RNA targets to show *ESR1* (blue points) and *FOXL2* (fast red points) RNAs (A2, B2), and *ESR1* (blue) and *OCT4* (fast red) RNAs (A3, B3). The lower panel is the fluorescence observation of the fast red *OCT4* ISH labeling, showing the overall density of *OCT4*-positive cells (A4, B4). The *ESR1/FOXL2* ISH image in the control ovary is the same as that presented in Fig. 6.

reduced *OCT4* gene expression by each cell, as previously suggested by the ISH analysis (Fig. 8). Interestingly, the expression of *WNT4* was significantly higher at 22 dpc in KO ovaries, suggesting that β-catenin signaling was stimulated in KO ovaries. The expression level of the *DDX4* gene, known to be low at this ovarian developmental stage (13), did not differ between WT and *ARO*$^{-/-}$. It increased between 20 and 22 dpc, as classically observed during ovary differentiation (13). Expression of the *SOX9* gene was 3 to 6 times lower in the ovaries of all genotypes than in testes at the same age. The SOX9 transcription factor was not detected by immunohistology in either WT or *ARO*$^{-/-}$ ovaries, while clear labeling was observed in the fetal testis at 22 dpc (Supplementary Figure 6 (29)). This reinforces the demonstration that *ARO*$^{-/-}$ ovaries did not display any sex reversal phenotype at early stages. The expression levels of the *ESR1* and *ESR2* genes did not change significantly.

Thus, from 20 dpc onwards, differentiation of the *ARO*$^{-/-}$ gonad was profoundly altered, with reduced thickness of the coelomic epithelium, and a weaker expression of the germ cell marker gene *OCT4* and of the somatic cell markers *FOXL2* and *RSPO1*. This ultimately led to a clearly underdeveloped small organ with small ovigerous nests, a spread of connective tissue beneath the surface epithelium and an abnormal layout of *FOXL2*-positive cells.

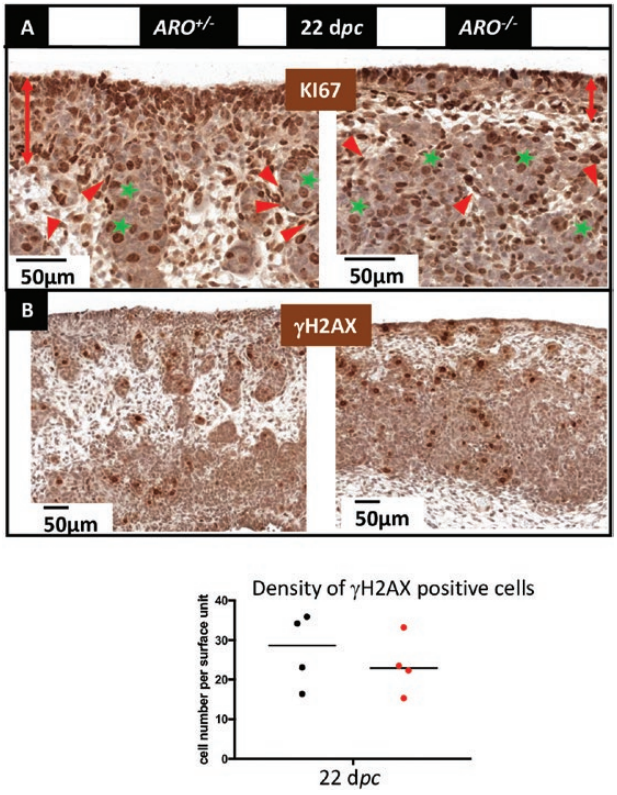

Figure 9. Mitotic activity and DNA fragmentation at 22 dpc. The marker of mitotic activity KI67 (A), and that of double-strand breaks γH2AX (B) were localized by immunohistochemistry in sections from PAF-fixed ovaries from *ARO*$^{+/-}$ and *ARO*$^{-/-}$ fetuses at 22 dpc. The KI67 antibody labeled the nuclei of most cells in the coelomic epithelium, and numerous cells inside the ovary in both genotypes. Cells with flat nuclei that were KI67-positive (red arrowheads) intermittently surrounded the ovigerous cords. Cells with large round nuclei that were positive for KI67 labeling (probably germ cells) were mainly found inside the cords (green stars). The red double arrow indicates the thickness of the surface epithelium enriched with KI67-positive cells. Expression of the KI67 gene did not differ in all the ovaries. The γH2AX antibody labeled large round shaped nuclei, probably corresponding to germ cells. Note the disconnection between the coelomic epithelium and the newly forming ovigerous cords in *ARO*$^{-/-}$ ovaries. The density of γH2AX-positive cells did not differ in wild-type and *ARO*$^{-/-}$ Ovaries.

Impact of Estrogen Deprivation on Germ Cell Meiosis and Follicular Differentiation

In the rabbit ovary, the first signs of meiosis are detected histologically at 30 to 31 dpc, ie, at around birth. Typical meiotic germ cells (prophase I) are then observed for less than 2 weeks. After meiosis arrest at diplotene stage, follicles start to differentiate. The peak of expression of the *STRA8* gene that marks the commitment of germ cells to meiosis starts at 24 to 28 dpc (13). We therefore sought to analyze at 28 dpc (meiosis commitment), 34 dpc (start of meiosis) and a few days or weeks after birth (folliculogenesis) whether the initiation and arrest of meiosis I and early follicular formation were impacted in *ARO*$^{-/-}$ ovaries.

In WT and *ARO*$^{-/-}$ 28 dpc ovaries (Fig. 11A), numerous germ cells were positively labeled by *OCT4*, *DDX4*, and *STRA8* ISH specific probes (Fig. 11B-11D). The *STRA8* labeling proves the overall commitment of germ cells in meiosis in WT and *ARO*$^{-/-}$ ovaries. However, in these later, the number of positive germ cells for the 3 probes was low. More, they were clustered in small ovigerous-like structures, while in WT ovaries they were all observed in large ovigerous cords. Positive *FOXL2*-labeled cells were also much less numerous in *ARO*$^{-/-}$ ovaries, as shown by the low numbers of hybridization labels. Nevertheless, some of these *FOXL2*-positive cells displayed a flattened shape and surrounded the small ovigerous-like structures embedding germ cells, as in WT ovaries (Fig. 11E).

At 34 dpc, in WT ovaries, most ovigerous cords were filled with numerous zygotene germ cells, thus showing that meiosis had started in the majority of germ cells (Fig. 12A and a1). By contrast, in *ARO*$^{-/-}$ ovaries, germ cells at zygotene were sparse (Fig. 12B and b1, b2).

Differentiation of the *ARO*$^{-/-}$ ovaries was further altered, as shown by the weak staining observed with *DDX4*, *STRA8*, *SPO11* and *FOXL2* probes. The expression of all studied marker genes was reduced, except that of the *WNT4* gene (Fig. 13). The ratios of *STRA8/DDX4* and *SPO11/DDX4* mRNA levels were lower in *ARO*$^{-/-}$ ovaries, suggesting that *DDX4*-positive germ cells expressing *STRA8* and *SPO11* genes, and thus undergoing meiosis, were less abundant in *ARO*$^{-/-}$ ovaries. As regard to the somatic marker genes *FOXL2*, *RSPO1*, the expression of these genes was seriously impaired in *ARO*$^{-/-}$ ovaries when that of *WNT4* was apparently not modified.

These differences then intensified further (Supplementary Figure 7 (29)). As meiosis progressed (10 days postpartum, dpp), zygotene, pachytene, and diplotene stages were observed simultaneously in WT ovaries. At the interface between the cortex and medulla, the large ovigerous cords broke down to form numerous early primordial follicles encompassing diplotene stage germ cells surrounded by a ring of flat pregranulosa cells. This was far from being observed in *ARO*$^{-/-}$ ovaries. Indeed, 7 days after birth, almost no germ cells at the zygotene or pachytene stages were detected; a small number of diplotene-like stage cells were nonetheless found, some surrounded by a discontinuous ring of somatic cells that could be assumed to be pregranulosa cells.

Later on at 16 to 19 dpp, gonad size was approximately half that seen in *ARO*$^{-/-}$ rabbits, displaying a thin cortex with a small number of primordial follicles (Fig. 14A). Ovigerous cords broke down in both WT and *ARO*$^{-/-}$ ovaries and follicles were isolated. However, in *ARO*$^{-/-}$ ovaries, the ring of pregranulosa cells surrounding the oocytes was frequently discontinuous and rare, well-developed primordial follicles were detected. *FOXL2* ISH labeling was very

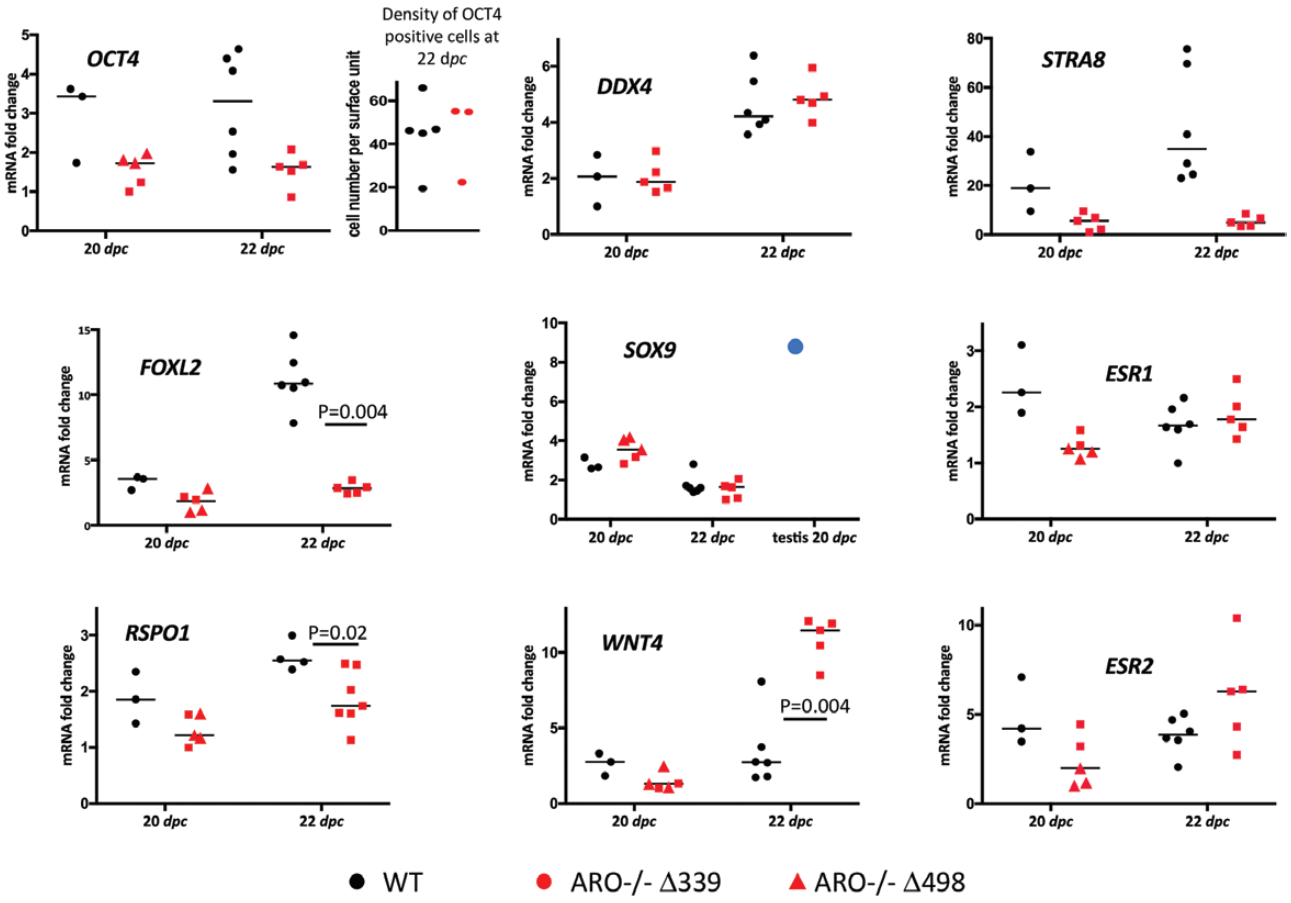

Figure 10. Gene expression in 20 and 22 dpc ovaries from wild-type (WT) and *ARO*$^{-/-}$ fetuses. Ovaries were collected from WT and mutant fetuses. The diagrams represent mRNA fold changes relative to the lowest point of each graph. Each point represents 1 RNA sample extracted from both gonads of 1 animal at the developmental stage indicated. The same RNA samples are analyzed in the 6 diagrams. Red triangles refer to mutants from the Δ339 line, and red points from the Δ829 line. No samples from the Δ498 line were analyzed. The blue point in the *SOX9* diagram shows the *SOX9* mRNA level measured in the 2 testes of 1 20 dpc WT fetus. Horizontal bars represent the medians. The density of cells positive for OCT4 is shown, together with the diagram showing expression of the *OCT4* gene.

weak, reflecting a low level of well-differentiated granulosa cells (Fig. 14B). Nevertheless, oocytes in primordial follicles were positive for the *RSPO2* ISH-specific probe in *ARO*$^{-/-}$ follicles, as in WT follicles (Fig. 14C).

To conclude, in *ARO*$^{-/-}$ ovaries, a small number of oocytes had differentiated after birth; these oocytes were surrounded by a ring of granulosa cells. Despite the probably abnormal differentiation of the latter (as shown by weak expression of the *FOXL2* gene), a small population of primordial follicles was able to differentiate. At the same time, the ovary was invaded by connective tissue filled with fibers rich in collagen, as previously observed from 20 dpc onwards; the latter was not replaced by ovigerous nests as normally occurs in nonmutant ovaries.

Discussion

The already longstanding demonstration of a peak of *CYP19A1* gene expression, AROMATASE activity and estradiol production by the fetal ovary in several mammal species between the stage of sex determination and the initiation of meiosis has raised questions regarding the effects of locally produced estrogens on the fetal differentiation of this organ. For many years, the mouse model was the only model available to study the function of genes in vivo. Strains of *Cyp19a1* gene or estrogen receptor gene KO mice were therefore created and a series of papers have reported their phenotype (39-44). All XX mice developed ovaries, but follicle differentiation was abnormal after birth. However, this model was not able to answer our question because the mouse is a species where *Cyp19a1* gene expression is detected after meiosis initiation in the "late" fetal ovary (45) and not before (46). Thanks to the recent possibility to target genome modifications in numerous other species, we created a rabbit model harboring a mutation in the *CYP19A1* gene (*ARO*$^{-/-}$), a species with a peak of *CYP19A1* gene expression in the fetal ovary before meiosis. *ARO*$^{-/-}$ rabbits were

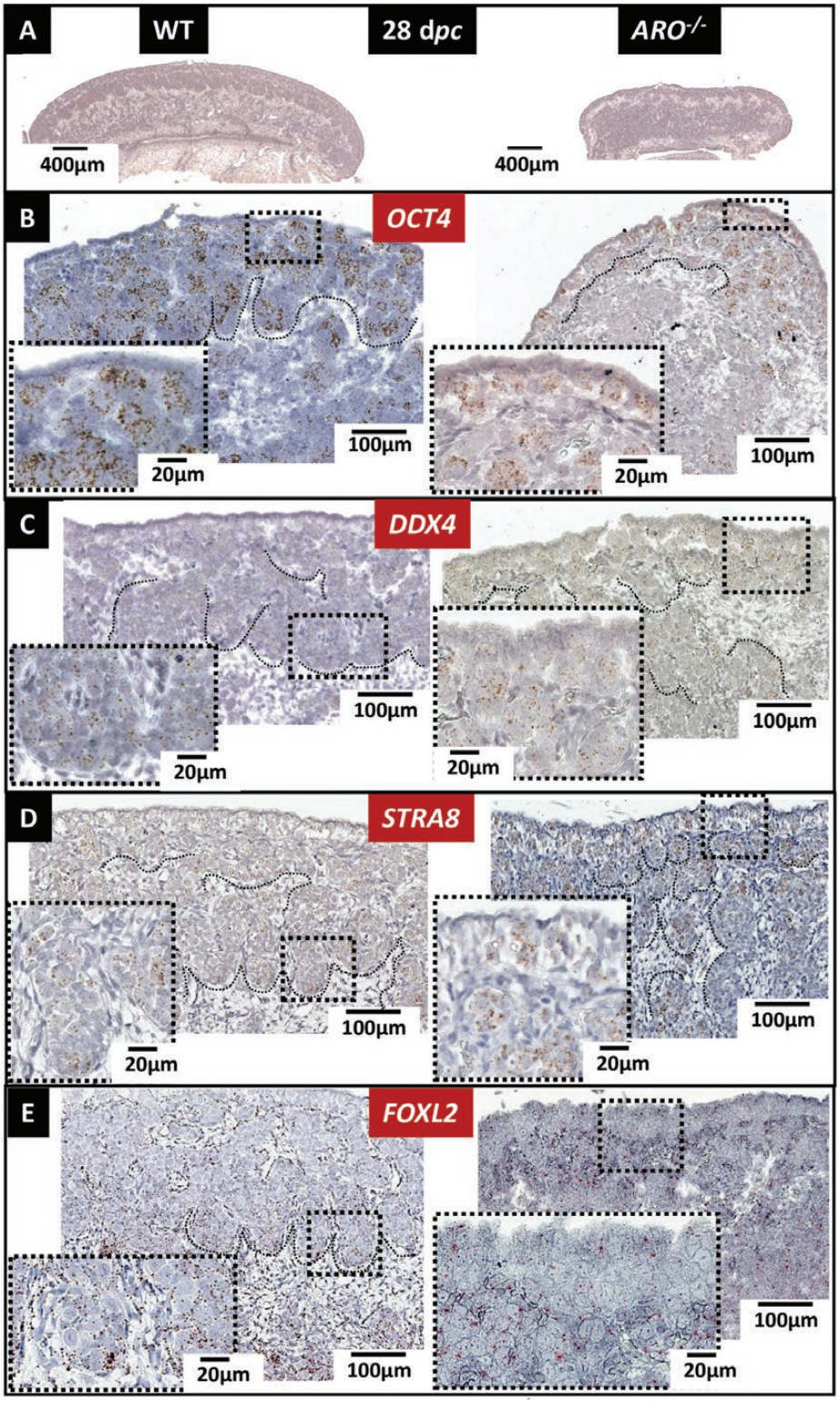

Figure 11. Germ cells were committed to meiosis in wild-type (WT) and *ARO*$^{-/-}$ ovaries from 28 dpc old fetuses. Ovaries were fixed in PAF, then HES stained or analyzed by ISH. (A) Morphology of the ovaries. The images show the difference in overall size of the gonads and the different thicknesses of the cortex. The *OCT4* (B) and *DDX4* (C) ISH probes labeled pluripotent germ cells and differentiating germ cells, respectively. The *STRA8* ISH probe (D) labeled germ cells committed to meiosis. The *FOXL2* ISH probe (E) labeled differentiating somatic cells. Note that the latter were mainly distributed around and within the ovigerous cords in WT ovaries, but in contrast were dispersed throughout the gonad in the *ARO*$^{-/-}$ rabbit. As in all ISH images, positive labeling appears as colored dots.

totally devoid of any estrogen production. In particular, estradiol levels in the gonads of all *ARO*$^{-/-}$ fetuses were undetectable, thus eliminating the possibility of any compensatory mechanism based on estradiol of maternal or

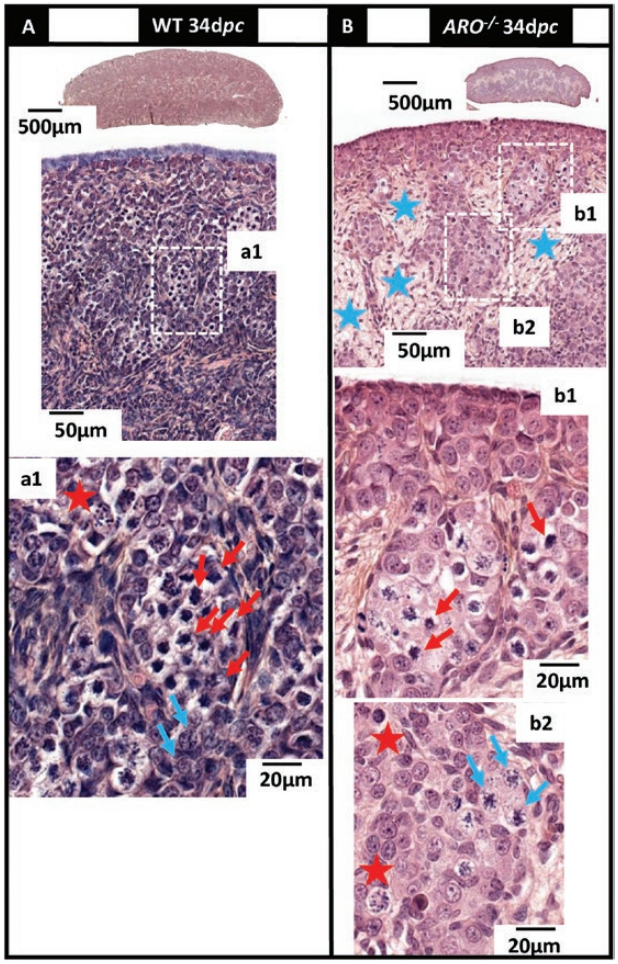

Figure 12. Meiosis in wild-type (WT) and *ARO*$^{-/-}$ ovaries. Ovaries collected at 34 dpc (3-4 days after birth) were fixed in Bouin's then HES stained. The stages of meiosis were identified as previously published (70). (A) In WT ovaries, large ovigerous cords were filled with numerous germ cells in zygotene (a1, red arrows). Few pachytene stages were observed in the inner part of the cords (a1, blue arrows). (B) In *ARO*$^{-/-}$ ovaries, the rare ovigerous cords were filled with a small number of germ cells in zygotene (b1). As in WT ovaries, some germ cells in pachytene were found in the inner part of the cords (b2). In both ovaries, aberrant pictures of cell nuclei were characterized by punctiform or condensed and dark colored chromatin (red stars). Blue stars indicate the connective tissue already observed, mostly in *ARO*$^{-/-}$ ovaries.

placental origins. Moreover, no testosterone was detected in *ARO*$^{-/-}$ fetal gonads, thus eliminating any interference due to a local accumulation of androgens in response to the lack of androgen aromatization. The key results of this study regarding the XX *ARO*$^{-/-}$ ovary phenotype were (1) no XX sex reversal in *ARO*$^{-/-}$ rabbits, (2) a small-sized ovary from early fetal stages because of low mitotic activity, (3) an abnormal layout of *FOXL2* positive cells, leading to the poor differentiation of ovigerous nests, and (4) a quasi-absence of follicular reserve, linked to the reduction in the number of meiotic germ cells and to the early failure of folliculogenesis.

AROMATASE Is Not an Ovarian-determining Enzyme in Mammals

Questions regarding the role of estrogens in mammalian sex determination were prompted by the finding that in goats, the *FOXL2* gene is a main actor in ovarian determination because *FOXL2* loss of function was found to cause ovary-to-testis sex reversal of the fetal gonad (6). FOXL2 had previously been shown to be a crucial transcriptional activator of the *CYP19A1* gene in goats (19) and fish (19, 26), and possibly in chicken (47). The question was therefore whether FOXL2 could act on sex determination through *CYP19A1* gene transcriptional activation. This question was all the more important in that in nonmammalian vertebrate species, anti-aromatase drugs can induce female to male sex reversal (see (25) in the chicken and (48) in fish). The rabbit was a potentially interesting model because, as in goats, the surge of *FOXL2* gene expression in the fetal ovary occurs when starts the peak of *CYP19A1* gene expression at the gonadal sex determination (13, 49). However, it should be noted that in contrast to what has already been published in goats (8), chickens (50), and fish (26), in rabbits, the 2 genes *CYP19A1* and *FOXL2* were predominantly expressed in different areas in the fetal ovary (Fig. 6). Therefore, if FOXL2 is an activator of *CYP19A1* transcription in the rabbit as it has been already published in the other species, a direct activation is unlikely. A series of studies should be necessary to confirm the localization of the expression of these genes and possibly the regulation pathways involved.

The results of the present study demonstrate that estrogens play no role in ovary/testis determinism in the rabbit gonad. A similar finding had already been described in humans, where several cases of homozygous *CYP19A1* gene mutations were reported (51-55). Despite numerous symptoms affecting the development of gonads, external genitalia and of breasts in girls, alongside multiple disorders affecting energy and bone metabolism, there was no evidence of sex reversal of the human ovary as regards genetic sex (51). Only virilization of the mother during pregnancy and of the external genitalia of the female fetus were reported and attributed to the inability of the placenta to aromatize androgens derived from the fetal adrenal glands (55). Contrasting data were reported in the mouse species, describing a rise in serum testosterone levels in *Cyp19a1*$^{-/-}$ females (39) and the presence of some seminiferous-like structures in the gonads of adult *Esr1/Esr2* double KO females (42, 56). The fact that this partial "sex reversal" phenotype had not been described in *Cyp19a1* KO mice suggests that suppressing the expression of estrogen receptors or suppressing their major ligand (in other words, estrogens) do not produce the same effects. It would be interesting to test whether such discrepancies also occur in

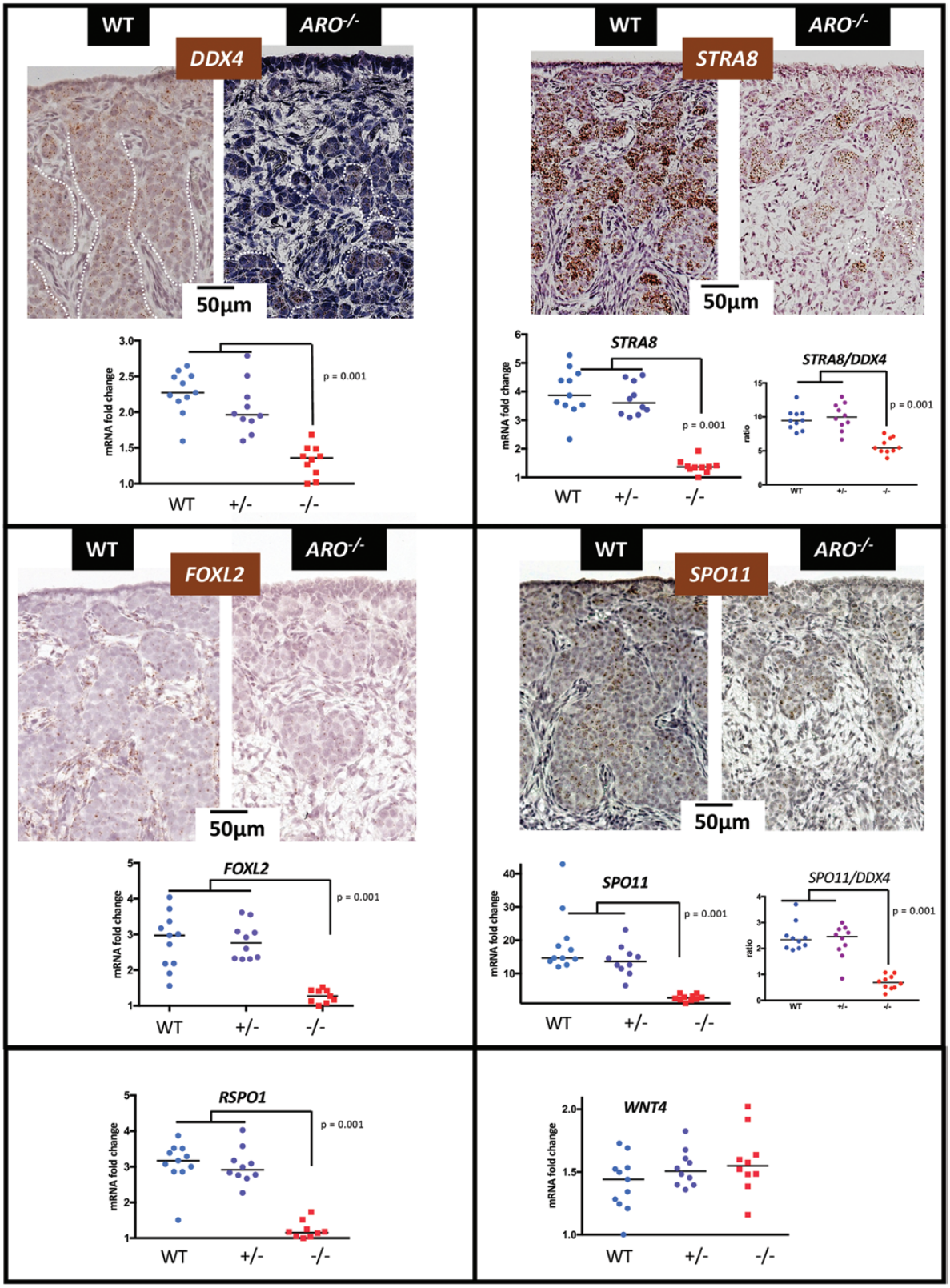

Figure 13. Expression of marker genes at meiosis. Germ cell marker genes (*DDX4*, *STRA8*, *SPO11*) and somatic cell marker genes (*FOXL2*, *RSPO1*, *WNT4)* were analyzed using ISH-specific probes and quantitative PCR. In wild-type ovaries, numerous germ cells positive for *DDX4*, *STRA8* and *SPO11* filled the ovigerous cords; *FOXL2*-positive pregranulosa cells were found around and within the cords. In *ARO*$^{-/-}$ ovaries, germ cells positive for these same ISH probes were also found but were much less numerous; the *FOXL2* labeling was very faint. The diagrams represent mRNA fold changes relative to the lowest point of each graph. Total RNA was extracted from the 2 gonads of each animal from wild-type (WT), *ARO*$^{+/-}$ (+/-) *and* *ARO*$^{-/-}$ (-/-) rabbits; the same RNA samples were analyzed in the diagrams. Horizontal bars represent the medians. As regard to the germ cell marker genes *STRA8* and *SPO11*, ratio to *DDX4* values are reported in the graphs on the right. Statistical significance ($P < .01$).

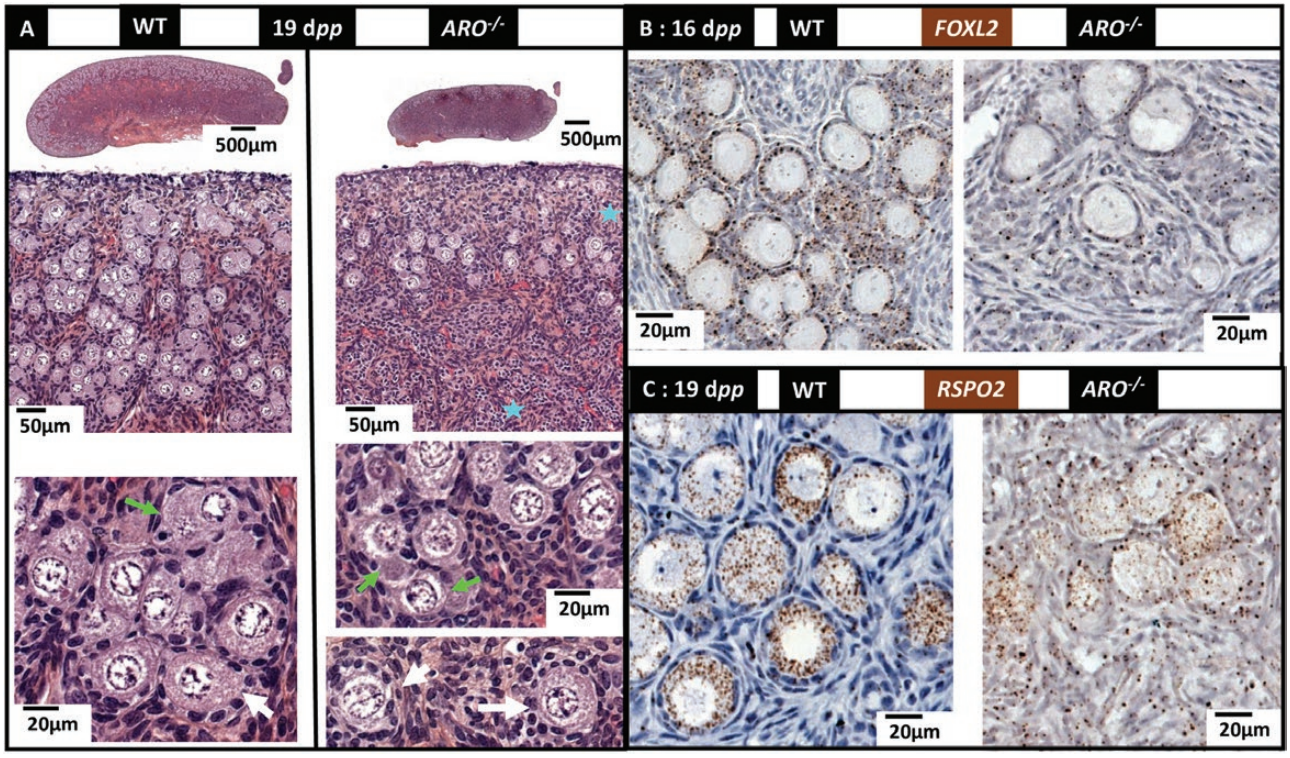

Figure 14. Early follicle differentiation. Ovaries were collected at 16 or 19 dpp then treated with Bouin's or PAF fixative and processed for HES staining or ISH labeling, respectively. (A) HES staining of 19 dpp sections. Blue stars indicate the abnormal persistence of connective tissue, devoid of differentiating oocytes or follicles, at the outer part of the cortex and in the medulla of *ARO*$^{-/-}$ ovaries. The green arrows highlight some of the primordial follicles in formation with a discontinuous wall of granulosa cells. Early formed primordial follicles surrounded by a wall of regular shape granulosa cells were found in wild-type (WT) and *ARO*$^{-/-}$ ovaries (white arrows). (B,C) ISH labeling using *FOXL2* and *RSPO2* gene specific probes. The *FOXL2* and *RSPO2* probes labeled granulosa cells and oocytes, respectively, in both WT and *ARO*$^{-/-}$ ovaries. Note the huge reduction in *FOXL2* positive cells in *ARO*$^{-/-}$ ovaries when compared with WT.

a nonrodent mammalian species. However, to our knowledge, double KO of the 2 estrogen receptor genes has never been achieved in such species, at least in rabbits.

Interestingly, the DMRT1 transcription factor was immunodetected at significant levels in granulosa cells from a small number of large antrum follicles in KO ARO ovaries from puberty. This does not negate the fact that estrogens play no role in the primary sex determination process but could be compared with what has been already reported in mice (57) and goats (8) concerning the rise in *DMRT1* expression in XX gonads after deletion of the *FOXL2* gene. To date, it has not been possible for us to conclude whether the presence of DMRT1 in the granulosa cells of KO ovaries is a direct effect of a lack of estrogens, or results from other induced modifications, such as a reduction of *FOXL2* gene expression. This needs to be further investigated using transcriptomic single cell analyses.

Estrogens Are Involved in Early Ovarian Differentiation

Fetal ovary differentiation is known to be intimately linked to mechanisms that involve cellular interactions and cell migration that are dependent on autocrine and paracrine signaling pathways. These processes involve genes coding for components of the extracellular matrix and cell–cell adhesion molecules. Estrogens have been reported as potent actors in these mechanisms (58-62). We have shown that the *CYP19A1* and *ESR1* genes were expressed by ovarian cortical cells and more specifically by cells located within the coelomic epithelium (Fig. 6 and Fig. 8A2). We can therefore hypothesize that in rabbit *ARO*$^{-/-}$ ovaries, the absence of estrogen can lead to a dramatic reduction of proliferative activity in the coelomic epithelium, as evidenced by KI67 staining (Fig. 9A). The decrease of *FOXL2* and *RSPO1* expression at 20 to 22 dpc (Fig. 10) might be related to a reduction in somatic cell numbers but also to an alteration in their differentiation. Overall, it results in a reduced size ovary, as detected shortly after gonadal sex determination.

A similar situation has already been described in chickens. Indeed, in this species, the experimental downregulation of the epithelial *Esrα* gene was sufficient to severely affect ovarian cortex differentiation (50). It was thus supposed that the natural absence of *Esrα* expression in the cortex of the right ovary of the hen was at least partially responsible for the asymmetric degeneration of the right ovary (63).

Other Mechanisms Are Likely to Compensate for the Lack of Estrogen

Notably, without estrogen, the proliferation of ovarian cells seemed to be affected but not abolished because some nests were clearly visible in *ARO*$^{-/-}$ gonads at birth although underdeveloped. Therefore, given that estrogens are involved in ovigerous nest formation other factors are also likely to play a role in this process. It has been shown in mice that the *Rspo1/Wnt4/β–catenin* pathway is involved in cell proliferation of the coelomic epithelium of both sexes during the gonadal switch (38). This pathway may thus be responsible, at least in part, for formation of the few ovigerous nests in *ARO*$^{-/-}$ rabbit ovaries. To support this hypothesis, we found that *WNT4* gene expression was significantly enhanced in the KO ovary (Fig. 10). This led us to suppose that in the absence of estrogen, gene pathways involving β-catenin signaling were overactivated in order to partially compensate for weak mitotic activity and to counter impairment of gonad differentiation. Transcriptomic studies at the single cell level should help to identify the cellular trajectories and better characterize such mechanisms.

The Number and Differentiation of Germ Cells Was Affected by the Lack of Estrogen

One of the main features of *ARO*$^{-/-}$ rabbit ovaries was the reduction in the total number of germ cells that was clearly visible from 20 to 22 dpc onwards. In mammals, germ cells colonize the genital crests at an early stage (58, 60, 62). In the rabbit, this starts at 9 dpc and is completed at around 18 dpc (64), when *CYP19A1* gene expression is initiated. Germ cell colonization thus occurs independently of *CYP19A1* expression. Therefore, in the *ARO*$^{-/-}$ ovary, the initial stock of germ cells was not altered.

In mammalian ovaries, the number of germ cells depends on both their mitotic activity (which is intense in the genital ridge) (57, 58) and on constant cell death, as has already been reported (59, 60). In the present study, cell death was unlikely to be the cause of the low germ cell count. Indeed, we did not observe stronger γH2AX labeling (which marks fragmentation of the DNA of cells in apoptosis) in KO and normal fetal ovaries. In contrast, mitotic activity may be involved. Indeed, in the rabbit, the mitotic activity of germ cells peaks at 16 to 18 dpc and remains high up to 26 dpc (56). This coincides with the strong expression of the *CYP19A1* and *ESR1* genes (Fig. 6). OCT4-positive germ cells were colocalized in the surface epithelium with cells expressing the *CYP19A1* and *ESR1* genes (Figs 6 and 8). Numerous articles have shown that in mammals, estradiol stimulates mitotic activity in the fetal ovary (57, 58). It is likely that the estradiol produced in situ by AROMATASE stimulates the mitotic activity of germ cells. Our data therefore suggest that it is probably not the death of germ cells but rather the absence of germ cell mitosis that was responsible for the small number of germ cells in the early ARO$^{-/-}$ ovary. Finally, the low level of *OCT4* gene expression in KO ovaries (and possibly the low germ cell expression) led us to suppose that germ cells suffer from compromised pluripotency from an early stage that may affect proliferation and/or meiotic entry time.

Germ Cells Were Committed to Meiosis Despite the Lack of Estrogens

The commitment of germ cells to meiosis marks the first step in their differentiation as oocytes. In the rabbit, this occurs during the third part of pregnancy (at around 28 dpc), and is characterized by the surge of *STRA8* gene expression, in germ cells specifically. Interestingly, in the *ARO*$^{-/-}$ ovaries, numerous germ cells were committed to meiosis as shown by the significant surge of *STRA8* gene expression; moreover, the various steps of meiotic prophase could be distinguished, and the meiosis-specific maker gene *SPO11* was also significantly expressed. This therefore suggests that neither estradiol nor the AROMATASE enzyme were necessary for meiotic induction and progression. As discussed previously, the number of germ cells that could be committed to meiosis was reduced in *ARO*$^{-/-}$ ovaries. Further, it should be pointed out that the ratio of *STRA8/DDX4* and *SPO11/DDX4* gene expression was low in *ARO*$^{-/-}$ ovaries, showing that an abnormal loss of germ cells occurred at commitment to, or during, meiosis. Therefore, although estrogens are not mandatory for meiosis commitment, the fact remains that they are important to limiting meiotic germ cell losses.

Estrogen Deprivation Impacts Follicle Formation

Another key feature of the phenotype of *ARO*$^{-/-}$ females concerned abnormal genital tract and ovarian follicle differentiation. At puberty, the genital tract of XX *ARO*$^{-/-}$ rabbits was profoundly altered, with massive atrophy, as previously reported in *Cyp19a1*$^{-/-}$ mice (39, 43) and in agreement with the fact already demonstrated that development of the female genital tract is highly estrogen dependent. The follicle differentiation that starts 12 to 15 days after birth in the rabbit at the arrest of meiosis prophase is a continuous process that involves the surrounding of oocytes with flat pregranulosa cells and the breakdown of ovigerous nests, thus giving rise to primordial follicles. The differentiation of pregranulosa cells from flat- to cuboidal-form cells then signals the differentiation

of primary follicles. Clearly, the size of the population of primordial follicles is linked to the number of oocytes, the latter being the consequence of all the events that occurred during fetal and neonatal life, as discussed previously. In the *ARO*$^{-/-}$ rabbit ovary, this is of particular importance because the pools of oocytes and of *FOXL2* expressing pregranulosa cells are extremely reduced. Moreover, it has been reported that the breakdown of nests is an event that is specifically sensitive to apoptotic losses (65). This could explain why the pool of primordial follicles was very low in *ARO*$^{-/-}$ rabbit ovaries 16 to 19 days after birth (Fig. 14) and almost null at puberty (Fig. 3). The weak expression of the *FOXL2* marker gene by granulosa cells 16 days after birth indicates the abnormal differentiation of primary follicles, the number of which was extremely low after puberty (Fig. 3). Surprisingly, controversial results have been reported in *Cyp19a1* KO mice, where the number of primary follicles was significantly higher than in WT mice (43). We do not yet have any explanation for such differences. Furthermore, we observed that despite the absence of estradiol, large antral follicles with oocytes developed in the *ARO*$^{-/-}$ ovary, although they were very few in number. This proves that estrogens are not the only actors in follicular growth and differentiation at puberty and after. Many previous studies have shown that these events are dependent on interactions between several signaling pathways, which include estrogens and also AMH and gonadotropins (66-68). Additional studies are under way to further analyze the mechanisms underlying the differentiation of these follicles in the absence of estradiol.

To conclude, the present work was able to show that in the rabbit, specific *CYP19A1* gene mutation and the absence of estrogens from early embryonic life were the source of a series of major disorders affecting the ovarian differentiation process. Two developmental stages were thus identified where the autocrine or paracrine activity of ovarian estrogens is crucial for ovarian differentiation: (1) a first stage during fetal life when estrogens act on proliferation and differentiation of cells from the coelomic epithelium and also on germ cells to achieve the formation of ovigerous nests, and (2) a second stage after birth and germ cell meiosis, when estrogens act on ovarian follicle formation. Our hypothesis is that the same applies in all other mammals when a long period with numerous mitoses intervenes between determinism of the sex of the gonad and the induction of meiosis, that is, in several mammal species but not in mice. This highlights the importance of the fetal period and thus shows why the maternal environment in these species can have a major impact, inducing irreversible effects. In addition, these data show that while estrogen therapy given after birth may have positive effects on development of the genital tract and metabolism, it cannot attenuate the effects of aromatase deficiency on early ovary differentiation.

Acknowledgments

The authors would like to thank staff at the facility (SAAJ, INRAE, Jouy-en-Josas) for their care of the rabbits, Julie Rivière and Marthe Vilotte (UMR GABI, INRAE, Jouy-en-Josas) for their assistance on the histology platform (@Bridge platform) and regarding access to the virtual slide scanner (MIMA2 platform), and Vicky Hawken for language corrections. Special thanks go to Danielle Monniaux (UMR PRC, INRAE, Nouzilly) for the time she spent in helpful discussions and offering very valuable comments.

Funding: This study was supported by ANR grants (GENIDOV:ANR-09-GENM-009; ARGONADS: ANR-13-BSV2-0017; ARDIGERM: ANR-2020-CE14), and the CELPHEDIA infrastructure (CELPHEDIA France, 2017).

Additional Information

Correspondence: Geneviève Jolivet, domaine de Vilvert, INRAE, 78350 Jouy-en-Josas, France. Email: genevieve.jolivet@inrae.fr.

Disclosures: The authors declare that they have no competing interests.

Data Availability: Some or all data generated or analyzed during this study are included in this published article or in the data repositories listed in References.

References

1. Sinclair AH, Berta P, Palmer MS, et al. A gene from the human sex-determining region encodes a protein with homology to a conserved DNA-binding motif. *Nature*. 1990;**346**(6281):240-244.
2. Gonen N, Futtner CR, Wood S, et al. Sex reversal following deletion of a single distal enhancer of Sox9. *Science*. 2018;**360**(6396):1469-1473.
3. Parma P, Radi O, Vidal V, et al. R-spondin1 is essential in sex determination, skin differentiation and malignancy. *Nat Genet*. 2006;**38**(11):1304-1309.
4. Chassot AA, Ranc F, Gregoire EP, et al. Activation of beta-catenin signaling by Rspo1 controls differentiation of the mammalian ovary. *Hum Mol Genet*. 2008;**17**(9):1264-1277.
5. Tomizuka K, Horikoshi K, Kitada R, et al. R-spondin1 plays an essential role in ovarian development through positively regulating Wnt-4 signaling. *Hum Mol Genet*. 2008;**17**(9):1278-1291.
6. Boulanger L, Pannetier M, Gall L, et al. FOXL2 is a female sex-determining gene in the goat. *Curr Biol*. 2014;**24**(4):404-408.
7. Pannetier M, Tilly G, Kocer A, et al. Goat SRY induces testis development in XX transgenic mice. *FEBS Lett*. 2006;**580**(15):3715-3720.
8. Elzaiat M, Jouneau L, Thépot D, et al. High-throughput sequencing analyses of XX genital ridges lacking FOXL2 reveal DMRT1 up-regulation before SOX9 expression during the sex-reversal process in goats. *Biol Reprod*. 2014;**91**(6):153.
9. Conley A, Hinshelwood M. Mammalian aromatases. *Reproduction*. 2001;**121**(5):685-695.

10. Dickmann Z, Dey SK, Gupta JS. Steroidogenesis in rabbit preimplantation embryos. *Proc Natl Acad Sci U S A*. 1975;**72**(1):298-300.
11. George FW, Wilson JD. Estrogen formation in the early rabbit embryo. *Science*. 1978;**199**(4325):200-201.
12. Gadsby JE, Heap RB, Burton RD. Oestrogen production by blastocyst and early embryonic tissue of various species. *J Reprod Fertil*. 1980;**60**(2):409-417.
13. Daniel-Carlier N, Harscoët E, Thépot D, Auguste A, Pailhoux E, Jolivet G. Gonad differentiation in the rabbit: evidence of species-specific features. *PLoS One*. 2013;**8**(4):e60451.
14. George FW, Milewich L, Wilson JD. Oestrogen content of the embryonic rabbit ovary. *Nature*. 1978;**274**(5667):172-173.
15. Gondos B, George FW, Wilson JD. Granulosa cell differentiation and estrogen synthesis in the fetal rabbit ovary. *Biol Reprod*. 1983;**29**(3):791-798.
16. Payen E, Pailhoux E, Abou Merhi R, et al. Characterization of ovine SRY transcript and developmental expression of genes involved in sexual differentiation. *Int J Dev Biol*. 1996;**40**(3):567-575.
17. Torley KJ, da Silveira JC, Smith P, et al. Expression of miRNAs in ovine fetal gonads: potential role in gonadal differentiation. *Reprod Biol Endocrinol*. 2011;**9**:2.
18. Mauleon P, Bezard J, Terqui M. Very early and transient 17β-estradiol secretion by fetal sheep ovary. In vitro study. *Ann Biol Anim Biochem Biophys*. 1977;**17**(3A):399-401.
19. Pannetier M, Fabre S, Batista F, et al. FOXL2 activates P450 aromatase gene transcription: towards a better characterization of the early steps of mammalian ovarian development. *J Mol Endocrinol*. 2006;**36**(3):399-413.
20. Ross DG, Bowles J, Hope M, Lehnert S, Koopman P. Profiles of gonadal gene expression in the developing bovine embryo. *Sex Dev*. 2009;**3**(5):273-283.
21. Shemesh M. Estradiol-17 beta biosynthesis by the early bovine fetal ovary during the active and refractory phases. *Biol Reprod*. 1980;**23**(3):577-582.
22. Garverick HA, Juengel JL, Smith P, et al. Development of the ovary and ontongeny of mRNA and protein for P450 aromatase (arom) and estrogen receptors (ER) alpha and beta during early fetal life in cattle. *Anim Reprod Sci*. 2010;**117**(1-2):24-33.
23. George FW, Wilson JD. Conversion of androgen to estrogen by the human fetal ovary. *J Clin Endocrinol Metab*. 1978;**47**(3):550-555.
24. Elbrecht A, Smith RG. Aromatase enzyme activity and sex determination in chickens. *Science*. 1992;**255**(5043):467-470.
25. Vaillant S, Dorizzi M, Pieau C, Richard-Mercier N. Sex reversal and aromatase in chicken. *J Exp Zool*. 2001;**290**(7):727-740.
26. Guiguen Y, Fostier A, Piferrer F, Chang CF. Ovarian aromatase and estrogens: a pivotal role for gonadal sex differentiation and sex change in fish. *Gen Comp Endocrinol*. 2010;**165**(3):352-366.
27. Lee JG, Sung YH, Baek IJ. Generation of genetically-engineered animals using engineered endonucleases. *Arch Pharm Res*. 2018;**41**(9):885-897.
28. Peyny M, Jarrier-Gaillard P, Boulanger L, et al. Investigating the role of BCAR4 in ovarian physiology and female fertility by genome editing in rabbit. *Sci Rep*. 2020;**10**(1):4992. Doi: 10.1038/s41598-020-61689-6
29. Jolivet G, Daniel-Carlier N, Harscoët E, et al. Supplementary information for: Fetal Estrogens are not involved in sex determination but critical for early ovarian differentiation in rabbits. https://data.inrae.fr/privateurl.xhtml?token=ab5db3bd-c712-4e9c-bc4c-09cf8562f71a
30. Sander JD, Cade L, Khayter C, et al. Targeted gene disruption in somatic zebrafish cells using engineered TALENs. *Nat Biotechnol*. 2011;**29**(8):697-698.
31. Jolivet G, Braud S, DaSilva B, et al. Induction of body weight loss through RNAi-knockdown of APOBEC1 gene expression in transgenic rabbits. *PLoS One*. 2014;**9**(9):e106655.
32. Giton F, Sirab N, Franck G, et al. Evidence of estrone-sulfate uptake modification in young and middle-aged rat prostate. *J Steroid Biochem Mol Biol*. 2015;**152**:89-100.
33. Devillers MM, Petit F, Cluzet V, et al. FSH inhibits AMH to support ovarian estradiol synthesis in infantile mice. *J Endocrinol*. 2019;**240**(2):215-228.
34. Bourdon M, Torres-Rovira L, Monniaux D, et al. Impact of a gestational exposure to diesel exhaust on offspring gonadal development: experimental study in the rabbit. *J Dev Orig Health Dis*. 2018;**9**(5):519-529.
35. Kaur J, Bose HS. Passenger protein determines translocation versus retention in the endoplasmic reticulum for aromatase expression. *Mol Pharmacol*. 2014;**85**(2):290-300.
36. Lee VH, Britt JH, Dunbar BS. Localization of laminin proteins during early follicular development in pig and rabbit ovaries. *J Reprod Fertil*. 1996;**108**(1):115-122.
37. Vainio S, Heikkilä M, Kispert A, Chin N, McMahon AP. Female development in mammals is regulated by Wnt-4 signalling. *Nature*. 1999;**397**(6718):405-409.
38. Chassot AA, Bradford ST, Auguste A, et al. WNT4 and RSPO1 together are required for cell proliferation in the early mouse gonad. *Development*. 2012;**139**(23):4461-4472.
39. Fisher CR, Graves KH, Parlow AF, Simpson ER. Characterization of mice deficient in aromatase (ArKO) because of targeted disruption of the cyp19 gene. *Proc Natl Acad Sci U S A*. 1998;**95**(12):6965-6970.
40. Findlay JK, Britt K, Kerr JB, et al. The road to ovulation: the role of oestrogens. *Reprod Fertil Dev*. 2001;**13**(7-8):543-547.
41. Hamilton KJ, Arao Y, Korach KS. Estrogen hormone physiology: reproductive findings from estrogen receptor mutant mice. *Reprod Biol*. 2014;**14**(1):3-8.
42. Couse JF, Hewitt SC, Bunch DO, et al. Postnatal sex reversal of the ovaries in mice lacking estrogen receptors alpha and beta. *Science*. 1999;**286**(5448):2328-2331.
43. Britt KL, Drummond AE, Cox VA, et al. An age-related ovarian phenotype in mice with targeted disruption of the Cyp 19 (aromatase) gene. *Endocrinology*. 2000;**141**(7):2614-2623.
44. Britt KL, Drummond AE, Dyson M, et al. The ovarian phenotype of the aromatase knockout (ArKO) mouse. *J Steroid Biochem Mol Biol*. 2001;**79**(1-5):181-185.
45. Dutta S, Mark-Kappeler CJ, Hoyer PB, Pepling ME. The steroid hormone environment during primordial follicle formation in perinatal mouse ovaries. *Biol Reprod*. 2014;**91**(3):1-12.
46. Greco TL, Payne AH. Ontogeny of expression of the genes for steroidogenic enzymes P450 side-chain cleavage, 3 beta-hydroxysteroid dehydrogenase, P450 17 alpha-hydroxylase/C17-20 lyase, and P450 aromatase in fetal mouse gonads. *Endocrinology*. 1994;**135**(1):262-268.
47. Govoroun MS, Pannetier M, Pailhoux E, et al. Isolation of chicken homolog of the FOXL2 gene and comparison of its

expression patterns with those of aromatase during ovarian development. *Dev Dyn*. 2004;**231**(4):859-870.
48. Yin Y, Tang H, Liu Y, et al. Targeted disruption of aromatase reveals dual functions of cyp19a1a during sex differentiation in zebrafish. *Endocrinology*. 2017;**158**(9):3030-3041.
49. Díaz-Hernández V, León del Río A, Zamora M, Merchant-Larios H. Expression profiles of SRY and SOX9 in rabbit gonads: the classical model of mammalian sex differentiation. *Sex Dev*. 2008;**2**(3):152-166.
50. Guioli S, Zhao D, Nandi S, Clinton M, Lovell-Badge R. Oestrogen in the chick embryo can induce chromosomally male ZZ left gonad epithelial cells to form an ovarian cortex that can support oogenesis. *Development*. February 25, 2020;**147**(4). Doi: 10.1242/dev.181693
51. Zhu WJ, Cheng T, Zhu H, et al. Aromatase deficiency: a novel compound heterozygous mutation identified in a Chinese girl with severe phenotype and obvious maternal virilization. *Mol Cell Endocrinol*. 2016;**433**:66-74.
52. Akçurin S, Türkkahraman D, Kim WY, Durmaz E, Shin JG, Lee SJ. A novel null mutation in P450 aromatase gene (CYP19A1) associated with development of hypoplastic ovaries in humans. *J Clin Res Pediatr Endocrinol*. 2016;**8**(2):205-210.
53. Unal E, Yildirim R, Tas FF, Demir V, Onay H, Haspolat YK. Aromatase deficiency due to a novel mutation in CYP19A1 gene. *J Clin Res Pediatr Endocrinol*. 2018;**10**(4):377-381.
54. Mazen I, McElreavey K, Elaidy A, Kamel AK, Abdel-Hamid MS. Aromatase deficiency due to a homozygous CYP19A1 mutation in a 46,XX Egyptian patient with ambiguous genitalia. *Sex Dev*. 2017;**11**(5-6):275-279.
55. Praveen VP, Ladjouze A, Sauter KS, et al. Novel CYP19A1 mutations extend the genotype-phenotype correlation and reveal the impact on ovarian function. *J Endocr Soc*. 2020;**4**(4):1-24.
56. Amano A, Kondo Y, Noda Y, et al. Abnormal lipid/lipoprotein metabolism and high plasma testosterone levels in male but not female aromatase-knockout mice. *Arch Biochem Biophys*. 2017;**622**:47-58.
57. Uhlenhaut NH, Jakob S, Anlag K, et al. Somatic sex reprogramming of adult ovaries to testes by FOXL2 ablation. *Cell*. 2009;**139**(6):1130-1142.
58. Juengel JL, Sawyer HR, Smith PR, et al. Origins of follicular cells and ontogeny of steroidogenesis in ovine fetal ovaries. *Mol Cell Endocrinol*. 2002;**191**(1):1-10.
59. Gentilini D, Busacca M, Di Francesco S, Vignali M, Viganò P, Di Blasio AM. PI3K/Akt and ERK1/2 signalling pathways are involved in endometrial cell migration induced by 17beta-estradiol and growth factors. *Mol Hum Reprod*. 2007;**13**(5):317-322.
60. Wilhelm D, Palmer S, Koopman P. Sex determination and gonadal development in mammals. *Physiol Rev*. 2007;**87**(1):1-28.
61. Zalewski A, Cecchini EL, Deroo BJ. Expression of extracellular matrix components is disrupted in the immature and adult estrogen receptor β-null mouse ovary. *PLoS One*. 2012;**7**(1):e29937.
62. Hummitzsch K, Irving-Rodgers HF, Hatzirodos N, et al. A new model of development of the mammalian ovary and follicles. *PLoS One*. 2013;**8**(2):e55578.
63. Guioli S, Nandi S, Zhao D, Burgess-Shannon J, Lovell-Badge R, Clinton M. Gonadal asymmetry and sex determination in birds. *Sex Dev*. 2014;**8**(5):227-242.
64. Chretien FC. [A study of the origin, migration and multiplication of the germ-cells of the rabbit embryo]. *J Embryol Exp Morphol*. 1966;**16**(3):591-607.
65. Myers M, Morgan FH, Liew SH, et al. PUMA regulates germ cell loss and primordial follicle endowment in mice. *Reproduction*. 2014;**148**(2):211-219.
66. Grynberg M, Pierre A, Rey R, et al. Differential regulation of ovarian anti-mullerian hormone (AMH) by estradiol through alpha- and beta-estrogen receptors. *J Clin Endocr Metab*. 2012;**97**(9):E1649-E1657.
67. Dewailly D, Robin G, Peigne M, Decanter C, Pigny P, Catteau-Jonard S. Interactions between androgens, FSH, anti-Müllerian hormone and estradiol during folliculogenesis in the human normal and polycystic ovary. *Hum Reprod Update*. 2016;**22**(6):709-724.
68. Chou CH, Chen MJ. The effect of steroid hormones on ovarian follicle development. *Vitam Horm*. 2018;**107**:155-175.
69. Bouraïma H, Hanoux V, Mittre H, Féral C, Benhaïm A, Leymarie P. Expression of the rabbit cytochrome P450 aromatase encoding gene uses alternative tissue-specific promoters. *Eur J Biochem*. 2001;**268**(16):4506-4512.
70. Kennelly JJ, Foote RH, Jones RC. Duration of premeiotic deoxyribonucleic acid synthesis and the stages of prophase I in rabbit oocytes. *J Cell Biol*. 1970;**47**(3):577-584.